Pore water geochemistry along continental slopes north of the East Siberian Sea: Inference of low methane concentrations

Clint M. Miller[1], Gerald R. Dickens[1], Martin Jakobsson[2], Carina Johansson[2], Andrey Koshurnikov[3], Matt O'Regan[2], Francesco Muschitiello[4], Christian Stranne[2], Carl-Magnus Mörth[2]

A revised manuscript submitted to:

Biogeosciences

[May 4, 2017]

[1]Department of Earth Science, Rice University, Houston, TX, USA

[2]Department of Geological Sciences, Stockholm University, Stockholm, Sweden

[3]V.I. Il'ichev Pacific Oceanological Institute, RAS

[4]Lamont-Doherty Earth Observatory, Columbia University, NY, USA

Correspondence to: Clint M. Miller (clint.m.miller@rice.edu)

Abstract: Continental slopes north of the Eastern Siberian Sea potentially hold large amounts of methane (CH_4) in sediments as gas hydrate and free gas. Although release of this CH_4 to the ocean and atmosphere has become a topic of discussion, the region remains sparingly explored. Here we present pore water chemistry results from 32 sediment cores taken during Leg 2 of the 2014 SWERUS-C3 expedition. The cores come from depth transects across the slope and rise extending between the Mendeleev and the Lomonosov ridges, north of Wrangel Island and the New Siberian Islands respectively. Upward CH_4 flux towards the seafloor, as inferred from profiles of dissolved sulfate (SO_4^{2-}), alkalinity, and the $\delta^{13}C$ of dissolved inorganic carbon (DIC), is negligible at all stations east of 143°E longitude. In the upper eight meters of these cores, downward sulfate flux never exceeds 6.2 mol/m^2-kyr, the upward alkalinity flux never exceeds 6.8 mol/m^2-kyr, and $\delta^{13}C$-DIC only slowly decreases with depth (-3.6‰/m on average). Moreover, upon addition of Zn acetate to pore water samples, ZnS did not precipitate, indicating a lack of dissolved H_2S. Phosphate, ammonium, and metal profiles reveal that metal oxide reduction by organic carbon dominates the geochemical environment, and supports very low organic carbon turnover rates. A single core on Lomonosov Ridge differs, as diffusive fluxes for SO_4^{2-} and alkalinity were 13.9 and 11.3 mol/m^2-kyr, respectively, the $\delta^{13}C$-DIC gradient was 5.6‰/m, and Mn^{2+} reduction terminated within 1.3 m of the seafloor. These are among the first pore water results generated from this vast climatically sensitive region, and they imply that abundant CH_4, including gas hydrates, do not characterize the East Siberian Sea slope or rise along the investigated depth transects. This contradicts previous modeling and discussion, which due to the lack of data are almost entirely based on assumption.

1. Introduction

41 The Arctic is especially sensitive to climate change, and has experienced anomalous
42 warming over the last century (Serreze et al., 2000; Peterson et al., 2002; Semiletov et al., 2004;
43 Polyakov et al., 2012). Past and future increases in atmospheric and surface water temperatures
44 should, with time, lead to significant warming of intermediate to deep waters (Dmitrenko et al.,
45 2008; Spielhagen et al., 2011), as well as sediment beneath the seafloor (Reagan and Moridis,
46 2009; Phrampus et al., 2014). Pore space within the upper few hundreds of meters of sediment
47 along many continental slopes contains temperature-sensitive methane (CH_4) in the form of gas
48 hydrates, free gas, and dissolved gas (Kvenvolden, 1993, 2001; Beaudoin et al., 2014).
49 Consequently, numerous papers have discussed the potential impact of future warming on CH_4
50 release from slope sequences of the Arctic Ocean (Paull et al., 1991; Reagan and Moridis, 2008;
51 McGuire et al., 2009; Biastoch et al., 2011; Elliott et al., 2011; Ferré et al., 2012; Giustiniani et
52 al., 2013; Thatcher et al., 2013; Stranne et al., 2016).
53 The amount and distribution of CH_4 in sediment along continental slopes remains poorly
54 constrained (Beaudoin et al., 2014). This is particularly true for the Arctic Ocean, because sea-
55 ice cover makes accessibility difficult. Nonetheless, numerous papers have inferred enormous
56 quantities of gas hydrate surrounding the Arctic (Kvenvolden and Grantz, 1990; Max and
57 Lowrie, 1993; Buffett and Archer, 2004; Klauda and Sandler, 2005; Max and Johnson, 2012;
58 Wallmann et al., 2012; Piñero et al., 2013; Fig. 1 and 2). In some sectors, compelling evidence
59 exists for abundant CH_4 and gas hydrate. Bottom simulating reflectors (BSRs) on seismic
60 profiles generally mark the transition between overlying gas hydrate and underlying free gas
61 (Holbrook et al., 1996; Pecher et al., 2001), and thereby imply high quantities of CH_4 in pore
62 space (Dickens et al., 1997; Pecher et al., 2001). Such BSRs have been documented along the
63 North Slope of Alaska (Collett et al., 2010), within the Beaufort Sea (Grantz et al., 1976; Grantz

et al., 1982; Weaver and Stewart, 1982; Hart et al., 2011; Phrampus et al., 2014), around Canadian Arctic Islands (Hyndman and Dallimore, 2001; Majorowicz and Osadetz, 2001; Yamamoto and Dallimore, 2008), adjacent to Svalbard (Posewang and Mienert, 1999; Hustoft et al., 2009; Petersen et al., 2010), and within the Barents Sea (Løvø et al., 1990; Laberg and Andreassen, 1996; Laberg et al., 1998; Ostanin et al., 2013). Furthermore, Lorenson and Kvenvolden (1995) observed high CH_4 concentrations in shelf waters of the Beaufort Sea, and Shakhova (2010a, 2010b) have documented CH_4 escape to the water column above the East Siberian shelf. Sediment on slopes north of the East Siberian Sea potentially contains copious CH_4 and gas hydrate (Fig. 1), although little data supports or refutes this hypothesis.

Regional assessments for abundant CH_4 in marine sediment along continental slopes can be acquired through two general approaches. The first includes geophysical applications, primarily seismic reflection profiling and the recognition of BSRs (Kvenvolden, 1993; Carcione and Tinivella, 2000; Haacke et al., 2008), which are a common, but not ubiquitous feature, of hydrate bearing sediments. The second utilizes chemical analyses of pore waters obtained from sediment cores (Borowski et al., 1999; D'Hondt et al., 2003). In marine sediments with abundant CH_4, a general process occurs near the seafloor. Microbes utilize upward migrating CH_4 and downward diffusing sulfate (SO_4^{2-}) via anaerobic oxidation of methane (AOM; Barnes and Goldberg, 1976; Boetius et al., 2000):

$$CH_4 + SO_4^{2-} \rightarrow HS^- + HCO_3^- + H_2O \quad (1)$$

The reaction leads to characteristic pore water chemistry profiles, with a clearly recognizable sulfate-methane transition (SMT; Fig. 3). The depth of the SMT inversely relates to the flux of CH_4, which in turns relates to the distribution of CH_4 beneath the seafloor (Borowski et al., 1999; Dickens, 2001; Bhatnagar, 2011). Where CH_4 fluxes toward the seafloor are high, the SMT is

located at shallow depth. For example, in cores from the continental shelf and slope of the Beaufort Sea, where seismic profiles indicate gas hydrate, Coffin et al. (2008, 2013) have documented SMTs in shallow sediment (< 10 mbsf).

The joint Swedish, Russian, U.S. Arctic Ocean Investigation of Climate-Cryosphere-Carbon interaction (SWERUS-C3) project is aimed at understanding spatial changes in carbon cycling across the continental margin north of Siberia. A central theme concerns the amount, distribution, and fluxes of CH_4. The overall project included a two-leg expedition in the boreal summer of 2014 using the Swedish icebreaker *IB Oden*. Between August 21 and October 5, Leg 2 sailed between Barrow, Alaska and Tromsø, Norway, including surveys of the continental slope of the East Siberian Sea. SWERUS Leg 2 included geophysical mapping and retrieval of numerous sediment cores, of which 446 pore water samples from eight piston, seven gravity, and 17 multicores (Fig. 2) were studied to ascertain potential fluxes of CH_4 toward the seafloor

2. Background

2.1 East Siberian margin geology

Extensive continental shelves and their associated slopes encircle the Arctic Ocean (Fig. 1). Although only 2.6% of the world's ocean by area (Jakobsson, 2002), the present Arctic Ocean receives ~10% of global freshwater input (Stein, 2008) as well as a massive discharge of terrigenous material (>249 Mt/yr; Holmes et al., 2002). Only Fram Strait (Fig. 1), with a modern sill depth of about 2540 m taken from the International Bathymetric Chart of the Oceans (IBCAO; Jakobsson et al., 2012), allows deep-water flow to and from the Arctic Ocean. It opened during the early to middle Miocene (Jakobsson et al., 2007; Engen et al., 2008; Hustoft et al., 2009). Prior to this, the Arctic Ocean was connected to other oceans only through shallow

seaways (e.g., Turgay Straight), such that deep waters may have been anoxic for long intervals of the Cretaceous and Paleogene (Moran et al., 2006; Sluijs et al., 2006; Jakobsson et al., 2007; O'Regan et al., 2011).

The East Siberian Sea stretches between Wrangel Island to the east and the New Siberian Islands to the west (Fig. 2). The continental shelf within this region is the widest in the world, extending 1500 km north of the coast. North of this expansive shelf lies the continental slope, which connects to Mendeleev Ridge to the east and Lomonosov Ridge to the west (Jakobsson et al., 2012). As these slopes lie north of the East Siberian Sea proper, we hereafter refer to them as SNESS for convenience.

2.2 Regional oceanography

Bottom waters impinging SNESS generally can be divided into three masses: the Pacific Halocline (~50-200m), the Atlantic Layer (~200-800m), and Canada Basin Bottom Water (>800m; Rudels et al., 2000). The Pacific Halocline is a cold (-1.5-0°C), low salinity (32-33.5 psu) water mass that serves as a boundary between sea ice and Atlantic Layer water (Aagaard, 1981; Aagaard and Carmack, 1989). The underlying Atlantic Layer is warmer (>0°C) but more saline (33.5-34.5 psu; Rudels et al., 2000). The Atlantic Layer originates from water arriving partly through Fram Strait and partly across the Barents Sea. Canada Basin Bottom Water is colder (~-0.5°C) and relatively saline (~34.9 psu), with a residence time exceeding 300 years (Stein, 2008). Importantly, inflow from the Atlantic varies over time, which can further influence temperature along slopes of the central Arctic Ocean (Dmitrenko et al., 2009).

2.3 Current speculation on gas hydrates in the Arctic

Even during summer months over the last decade, 2-3 m of sea ice covers much of SNESS (Stroeve et al., 2012). This necessitates the use of large ice breaking vessels to explore the region. Prior to SWERUS, only four icebreaker expeditions, the 1995 Polarstern Expedition ARK-XI/1 (Rachor, 1995), the 1996 Arctic Ocean Expedition ARK-XII/1 (Augstein et al., 1997), the 2008 Polarstern Expedition ARK-XXIII/3 (Jokat, 2010), and the 2009 Russian-American RUSALCA Expedition (Bakhmutov et al., 2009) have retrieved geophysical data and sediment on or adjacent to SNESS. So far, no deep drilling has occurred along SNESS. However, the 2004 Arctic Coring Expedition (Backman et al., 2009) drilled and cored the central Lomonosov Ridge (Fig. 1).

Despite the paucity of ground-truth data, many researchers have predicted widespread and abundant CH_4 within SNESS, as clearly shown by maps of inferred Arctic gas hydrate distribution (Fig. 1). This inference has arisen for two main reasons. First, the integrated input of particulate organic carbon (POC) over time provides the ultimate source of CH_4 in marine sediments (Kvenvolden and Grantz, 1990). Arctic slopes may contain high POC contents, which accumulated in a) shallow platform environments prior to the opening of the Amerasian Basin, (Spencer et al., 2011) b) during periods of high surface water productivity and oxygen poor bottom water conditions that persisted across much of the Arctic until the opening of the Fram Strait in the Neogene (Jakobsson et al., 2007; Stein, 2006; O'Regan et al., 2011; Jokat and Ickrath, 2015), or c) As terrigenous material carried to or deposited along the slopes during interglacial intervals of the Quaternary (Danyushevskaya et al., 1980; Darby, 1989; Archer, 2015). Certainly, organic rich Cretaceous and Eocene sediments have been documented on other Arctic margins and in the ACEX cores on Lomonosov Ridge (Moran et al., 2006; Backman and Moran, 2009; O'Regan et al., 2011). The second reason is that the thickness of the gas hydrate

156 stability zone (GHSZ) depends on bottom water temperature and the geothermal gradient
157 (Dickens, 2001). Because of very low bottom water temperatures along the slope, and generally
158 low regional geothermal gradients (O'Regan et al., 2016), an extensive volume of sediment can
159 host gas hydrate (Miles, 1995; Makogon, 2010).
160
161 *2.4 Pore water chemistry above methane-charged sediment*
162 Pore water chemistry provides powerful means to constrain CH_4 abundance and fluxes in
163 marine sediment (Borowski et al., 1996; Berg et al., 1998; Jørgensen et al., 2001; Torres and
164 Kastner, 2009; Treude et al., 2014). At locations without significant fluid advection, pore water
165 profiles relate to Fick's law of diffusion and chemical reactions (e.g., Berner, 1977; Froelich et
166 al., 1979; Klump and Martens 1981; Boudreau, 1997; and Iverson and Jorgensen, 1993). The
167 flux (J) of a dissolved species through porous marine sediment can be calculated from the
168 concentration gradient by (Li & Gregory, 1974; Berner, 1975; Lerman, 1977):
169 $$J = -\varphi D_s \frac{\partial C}{\partial Z}, \quad (2)$$
170 where φ is porosity, D_s is the diffusivity of an ion in sediment at a specified temperature, C is
171 concentration, and Z is depth. Note that, as generally written, J is positive for upward fluxes and
172 negative for downward fluxes relative to the seafloor.
173 At many locations, φ and D_s change only moderately (<20%) in the upper tens of meters
174 below the seafloor. However, abundant CH_4 in sediment leads to a large concentration gradient
175 toward the seafloor and, an upward flux of CH_4. The consequent reaction with SO_4^{2-} via AOM
176 (Eqn. 1) leads to a series of flux changes in dissolved components (addition or removal), and
177 predictable variations in concentration profiles across an SMT (Alperin, 1988; Borowski et al.,
178 1996; Niewohner et al., 1998; Ussler and Paull, 2008; Dickens and Snyder, 2009; Chatterjee et

al., 2011). Furthermore, the depth of the SMT directly relates to the flux of CH_4 from below (Jørgensen et al., 1990; Dickens, 2001; D'Hondt et al., 2002; Hensen et al., 2003), largely because SO_4^{2-} concentrations at the seafloor are nearly constant throughout the oceans.

Large areas of continental slopes across the world host CH_4 in sediment, and consequently have a prominent SMT (D'Hondt et al., 2002). This feature is generally within the upper 30 m beneath the seafloor, and is characterized as a thin (<3 m) horizon with major inflections in both CH_4 and SO_4^{2-} profiles (Fig. 3). Sulfate concentrations decrease from seawater values at the seafloor to zero at the SMT; by contrast, CH_4 concentrations rise from zero at the SMT to elevated values at depth.

Importantly, though, as one can infer from Eqns. 1 and 2, AOM affects additional species dissolved in pore water (Alperin et al., 1988; Jørgensen et al., 1990; Dickens, 2001; Hensen et al., 2003; Snyder et al., 2007). Dissolved HS^- and HCO_3^- concentrations necessarily increase across the SMT, so an inflection occurs in their concentration profiles. These two species contribute to total alkalinity of marine waters (Gieskes and Rogers, 1973; Haraldsson et al., 1997), which can be defined as:

$$Alk_T = [HCO_3^-] + 2[CO_3^{2-}] + [HS^-] + [B(OH)_4^-] + [OH^-] + [HPO_4^{2-}] + [NH_3] + [X] , \quad (3)$$

where X refers to several minor species. However, in shallow sediments found above almost all CH_4 charged systems, this can be expressed as:

$$Alk_T \approx [HCO_3^-] + [HS^-] . \quad (4)$$

Therefore, because of the production of HS^- and HCO_3^-, an inflection in Alk_T occurs across the SMT (Luff and Wallmann 2003; Dickens and Snyder, 2009; Jørgensen and Parkes, 2010; Chatterjee et al., 2011; Smith and Coffin, 2014; Ye et al., 2016).

Marked changes in pore water profiles of other components also typically occur across the SMT (Fig. 3). Because CH_4 is greatly depleted in ^{13}C, due to isotope fractionation during methanogenesis at depth (Whiticar, 1999; Paull et al., 2000), the conversion of CH_4 to HCO_3^- (Eqn. 1) decreases the $\delta^{13}C$ of DIC across the SMT (Torres et al., 2007; Holler et al., 2009; Chatterjee et al., 2011; Yoshinaga et al., 2014). However, the magnitude of this change in $\delta^{13}C$-DIC is complicated because excess ^{13}C-enriched HCO_3^- (formed during methanogenesis and subsequent reactions) can also rise from below (Snyder et al., 2007; Chatterjee et al., 2011). Dissolved Ba^{2+} concentrations generally increase significantly just above the SMT. This is because solid barite ($BaSO_4$), a ubiquitous component of marine sediment on continental slopes (Dymond et al., 1992; Gingele and Dahmke, 1994), dissolves in the SO_4^{2-}-depleted pore water and dissolved Ba^{2+} then diffuses back across the SMT (Dickens, 2001; Riedinger et al., 2006; Nöthen and Kasten, 2011). Dissolved Ca^{2+} concentrations usually decrease across the SMT. This is due to authigenic carbonate precipitation resulting from the production excess HCO_3^- (Greinert et al., 2001; Luff and Wallmann 2003; Snyder et al., 2007). Conversely, dissolved NH_4^+ concentrations exhibit no inflection across the SMT. This is because while decomposition of particulate organic matter (POM) generates NH_4^+, AOM does not (Borowski et al., 1996).

Studies at numerous locations demonstrate that characteristic pore water profiles delineate sediment sequences with significant CH_4, including gas hydrate, in the upper few hundred meters below the seafloor (Fig. 3). Good examples include: Baltic Sea (Jørgensen et al, 1990), Black Sea (Jørgensen et al, 2004), Blake Ridge (Paull et al., 2000; Borowski et al., 2001), Cariaco Trench (Reeburgh, 1976), Cascadia Margin (Torres and Kastner, 2009), Gulf of Mexico (Kastner et al., 2008a; Hu et al., 2010; Smith and Coffin, 2014), Hydrate Ridge (Claypool et al., 2006), offshore Namibia (Niewohner et al., 1998), offshore Peru (Donohue et al., 2006), South China

225 Sea (Luo et al., 2013; Hu et al., 2015), and Sea of Japan (Expedition Scientists, 2014). Moreover,
226 in regions dominated by diffusion, fluxes of dissolved CH_4 can be estimated using Eqn. 2 from
227 concentration profiles of multiple constituents (e.g., SO_4^{2-}, HCO_3^-, Ca^{2+}) and knowledge of
228 porosity and sedimentary diffusion constants (e.g., Niewohner et al., 1998; Snyder et al., 2007).
229 At sites with abundant CH_4 in the upper few hundred meters below the seafloor, notably
230 including sites with gas hydrate and sites in the Beaufort Sea, estimated values for $J CH_4$ and -
231 $J SO_4^{2-}$ are universally high (> ~50 mol/m^2-kyr).
232 It should be noted that, at seafloor locations with significant upward advection of fluids,
233 such as at seeps and vents, the aforementioned reactions occur, but the pore water profiles
234 become more complicated to model (Berner, 1980; Torres et al., 2002; Chatterjee et al., 2014).
235 This is because the advecting fluids typically have different chemistry than surrounding sediment
236 (even if charged with CH_4), and because advection often involves multiphase fluid flow (free gas
237 and liquid) that may be episodic. Nonetheless, at least on continental slopes, if the upward
238 advecting fluids contain significant CH_4 (even as gas bubbles), a prominent SMT occurs, but is
239 shoaled toward the seafloor with respect to predictions based on CH_4 diffusion alone (Luff and
240 Wallmann, 2003; Kastner et al., 2008a). Indeed, at locations where CH_4 gas bubbles escape the
241 seafloor, the SMT lies at the seafloor (e.g., Aharon and Fu, 2000; Joye et al., 2004; Hu et al.,
242 2010).
243
244 **3. Materials and Methods**
245 *3.1 SWERUS-C3 Expedition, Leg 2*
246 Leg 2 of SWERUS-C3 included four transects across the SNESS (Fig. 2). These transects
247 were along Arlis Spur (TR-1), north of central East Siberia (TR-2), from close to Henrietta

Island to the Makarov Basin (TR-3), and on the Amerasian side of Lomonosov Ridge (TR-4). Along each transect, scientific operations involved bathymetric mapping as well as sediment coring at stations. An additional coring station was located on Lomonosov Ridge, near its intersection with the Siberian margin.

An array of coring techniques were used along each transect. In total, 50 sediment cores were collected at 34 stations. These included: multicore sets (22), gravity cores (23), piston cores (11), and kasten cores (2). The multicorer was an 8-tube corer built by Oktopus GmbH. The polycarbonate liners were 60 cm long with a 10 cm diameter. The piston/gravity coring system was built by Stockholm University with an inner diameter of 10 cm. Trigger weight cores also were collected during piston coring. The different coring systems enabled sediment and pore water collection from the seafloor to upwards of 9 m below the seafloor (mbsf).

3.2 Core material

For gravity and piston cores, physical properties were analyzed on the ship using a Geotek Multi-Sensor Core Logger (MSCL). These included measurements of the gamma-ray derived bulk density, compressional wave velocity (p-wave), and magnetic susceptibility at 1 cm resolution. Discrete samples (2-3 per section) were taken for sediment index property measurements (bulk density, porosity, water content and grain density). Grain density was measured using a helium displacement pycnometer on oven-dried samples. Porosity profiles were generated using the smoothed (3-pt) MSCL-derived bulk density (ρ_B) and the average grain density (ρ_g) from each core, where

$$\varphi = \frac{(\rho_g - \rho_b)}{(\rho_b - \rho_f)}, \quad (5)$$

and the pore fluid density (ρ_f) was assumed to be 1.024 g/cm^3.

271

272 *3.3 Interstitial water collection*

273 Cores were cut into ~1.5 m long sections immediately on the ship deck, brought to the
274 geochemistry laboratory, and placed on precut racks. Laboratory temperature was a near constant
275 22 °C. Pore waters were collected using Rhizon samplers (Seeberg-Elverfeldt et al., 2005;
276 Dickens et al., 2007). Sampling involved drilling holes through the core liner, inserting Rhizons
277 into the sediment core, and obtaining small volumes of pore water via vacuum and
278 "microfiltration." The Rhizons used were 5-cm porous flat tip male luer lock (19.21.23) with 12
279 cm tubing, purchased from Rhizosphere Research Products (www.rhizosphere.com).

280 In total, 529 pore water samples were collected from 32 cores, which ranged from 0.16 to
281 8.43 m in length (Tbl. S2). Rhizons in gravity and piston cores typically were spaced every 20 to
282 30 cm. Because the use of rhizon sampling for collecting pore waters of deep-sea sediments
283 remains a relatively novel and engaging topic (Dickens, 2007; ; Xu et al., 2012; Miller et al.,
284 2014), we discuss the procedure, as well as several experiments regarding our sampling, in
285 Supplementary Information.

286 While in the shipboard laboratory, Rhizon samples were divided into six aliquots when
287 sufficient water was available. This sample splitting led to 2465 aliquots of pore water in total,
288 which then could be examined for different species at different laboratories. Aliquots 1, 3, and 6
289 (below) were collected for all 32 cores.

290

291 *3.4 Interstitial water analyses*

292 The first aliquot was used to measure total alkalinity using a Mettler Toledo titrator
293 onboard *IB Oden*. Immediately after collection, pore water was diluted with milli-Q water and

294 autotitrated. Fifteen spiked samples and eight duplicates were analyzed onboard for quality
295 control. Spiked samples were created by pipetting certified reference material (Batch 135;
296 www.cdiac.ornl.gov/oceans/Dickson_CRM) into milli-Q water. Results for spiked samples and
297 duplicates are reported in Tbl. 1.

298 The second aliquot was used to measure the $\delta^{13}C$ composition of DIC ($\delta^{13}C$-DIC). Septum
299 sealed glass vials prepared with H_3PO_4 and flushed with helium were prepared before the
300 expedition. Samples were sealed in boxes and refrigerated for the remainder of the cruise. Four
301 field duplicates, two seawater standards, and a field blank were collected, stored, and analyzed
302 with the samples. The $\delta^{13}C$-DIC analyses were performed on a Gasbench II coupled to a MAT
303 253 Mass Spectrometer (both Thermo Scientific) at Stockholm University. The $\delta^{13}C$-DIC is
304 reported in conventional delta notation relative to Vienna PeeDee Belemnite (VPDB). Results
305 for field duplicates and standards are reported in Tbl. 1. Standard deviation for the analyses of
306 $\delta^{13}C$-DIC was less than 0.1 ‰.

307 The third aliquot was used to measure dissolved sulfur and metal concentrations. Samples
308 were acid preserved with 10 µL ultrapure HNO_3. Additionally, 11 blind field duplicates and 2
309 field blanks were collected and processed in the same manner. Concentrations of Ba, Ca, Fe, Mg,
310 Mn, S, and Sr were determined on an Agilent Vista Pro Inductively Coupled Atomic Emission
311 Spectrometer (ICP-AES) in the geochemistry facilities at Rice University. Known standard
312 solutions and pore fluid samples were diluted 1:20 with 18-MΩ water. Scandium was added to
313 both standards and samples to correct for instrumental drift (emission line 361.383 nm).
314 Wavelengths used for elemental analysis followed those indicated by Murray et al. (2000).
315 Following initial analysis, an additional dilution, 1:80 with 18-MΩ water, was analyzed for Ca,
316 Mg, and S. After every 10 analyses, an International Association of Physical Sciences (IAPSO)

317 standard seawater spiked sample and a blank were examined for quality control. Relative
318 standard deviations (RSD) from stock solutions are reported in Tbl. 1.

319 The fourth aliquot was used to measure dissolved ammonia (NH_4^+) via a colorimetric
320 method similar to that presented by Gieskes et al. (1991). Set volumes of pore water were
321 pipetted into cuvettes and diluted with milli-Q water. Two reagents were then pipetted into the
322 cuvettes. Reagent A was prepared by adding $Na_3C_6H_5O_7$, C_6H_5OH, and $Na_2(Fe(CN)_5NO)$ to
323 milli-Q water. Reagent B was prepared by dissolving NaOH in milli-Q water and adding NaClO
324 solution. Solutions were mixed and allowed to react for at least six but not more than 24 hours.
325 Solutions turned various shades of blue, which to relate to NH_4^+ concentration, and were
326 measured by absorbance at 630 nm on a Hitachi U-1100 spectrophotometer. Five point
327 calibration curves were measured before each sample set and corrected using VKI standard (QC
328 RW1; www.eurofins.dk; Tbl. 1).

329 The fifth aliquot was used to measure dissolved phosphate (PO_4^{3-}) following the method
330 given by Gieskes et al. (1991). Remaining pore water (generally between 1 and 3mL) was added
331 to milli-Q water to a sum of 10 mL. Two reagents were added to the solution to react with PO_4^{3-}.
332 Reagent A was prepared by making three solutions: $(NH_4)_2MoO_4$, H_2SO_4, and $C_8H_4K_2O_{12}Sb_2 \bullet$
333 XH_2O were added to milli-Q water, and the solutions were added dropwise. Reagent B was
334 created with $C_6H_8O_6$. After samples were prepared, reagents A and B were added, mixed, and
335 allowed to react 30 minutes. Solutions turned various shades of blue, relating to PO_4^{3-}
336 concentration, and were measured at an absorbance of 880 nm. Five point calibration curves
337 were measured before each sample set and corrected using VKI standard (QC www.eurofins.dk;
338 Tbl. 1).

For 352 pore water samples, a sixth aliquot of approximately 2 mL was mixed with 200 µL of a 2.5% Zn-acetate ($Zn(C_2H_3O_2)_2$) solution. Given the extremely low solubility of ZnS, a white precipitate forms when such a solution is added to pore water samples with even trace H_2S concentrations (Cline, 1969; Goldhaber, 1974).

For the ICP-AES analyses, a method detection limit (MDL) can be determined as follows:

$$MDL = \left(\frac{C_{High} - C_{Low}}{I_{High} - I_{Low}}\right) 3\sigma \,, \quad (6)$$

where C = concentration and I = intensity (counts per second on the ICP-AES). The MDLs were as follows: Ba = 0.01 µM, Ca = 0.08 µM, Fe = 5.9 µM, Mg = 0.22 µM, Mn = 0.24 µM, S = 1.2 µM, Sr = 0.01 µM. On all plots, for reference, we place dashed lines for values of the IAPSO seawater standard (Alkalinity = 2.33 mM, Ba = 0.00 mM, Ca = 10.28 mM, Fe = 0.00 mM, Mg = 53.06 mM, Mn = 0.00 mM, S = 28.19 mM, Sr = 0.09 mM, NH_4 = 0.00 mM, HPO_4 = 0.00 mM).

4. Results

4.1 General observations

With the large number of pore water measurements (Tbl. S1), we begin with some generalities regarding results. We plot pore water concentration profiles along each transect collectively (Fig. 4-8), irrespective of coring device or water depth, although clear variance in pore water chemistry exists between stations for some dissolved species (e.g., Fe).

Most species display "smooth" concentration profiles with respect to sediment depth (Fig. 4-8). That is, concentrations of successive samples do not display a high degree of scatter. This is expected for pore water profiles in sediment where diffusion dominates (Froelich et al., 1979; Klump and Martens 1981; Schulz, 2000; Torres and Kastner, 2009; Hu et al., 2015). However, for some dissolved species whose concentrations do not appreciably change over depth (e.g.,

362 Ba^{2+} and Ca^{2+}), scatter exists beyond that predicted from analytical precision. We discuss this in
363 the Supplementary Information.
364
365 *4.2 Alkalinity and $\delta^{13}C$ of DIC*
366 Alkalinity concentrations increase with depth in all cores (Fig. 4-8). Moreover, in most
367 cases, the rise is roughly linear. Across all stations on the four transects, alkalinity increases by
368 an average of 0.51 mM/m, although variance exists between mean gradients for each transect
369 (Tr1 = 0.46 mM/m, Tr2 = 0.34 mM/m, Tr3 = 0.91 mM/m, and Tr4 = 0.44 mM/m) and by station
370 along each transect. The Lomonosov Ridge station differs (Fig. 8), as alkalinity increases much
371 greater with depth (1.86 mM/m).
372 Concave-down $\delta^{13}C$-DIC profiles characterize pore waters at all stations (Fig. 4-8). The
373 decrease in $\delta^{13}C$-DIC is most pronounced near the seafloor. Across all stations along the four
374 transects, pore water $\delta^{13}C$-DIC values decrease from near zero close to the mudline at an average
375 of -3.6 ‰/m. Again, variance in mean gradients occurs between stations and transects (Tr1 = -
376 3.3 ‰/m, Tr2 = -3.0 ‰/m, and Tr3 = -4.7 ‰/m). As with alkalinity, the $\delta^{13}C$-DIC profile at the
377 Lomonosov Ridge station differs, with values decreasing by 5.6 ‰/m, such that by eight mbsf,
378 $\delta^{13}C$-DIC approaches -45 ‰. In summary, a basic relationship exists between higher alkalinity
379 and lower $\delta^{13}C$-DIC across all stations.
380
381 *4.3 Sulfur and sulfate*
382 No sulfide was observed by smell and no ZnS precipitated in any pore water sample upon
383 addition of Zn-acetate solution. Molar concentrations of total dissolved sulfur should, therefore,
384 represent those of dissolved SO_4^{2-}. Along the four transects, dissolved S concentrations decrease

with depth at all stations (Fig. 4-7). The total dissolved S concentrations in the shallowest samples varied from 27.3 to 30.6 mM and averaged 28.7 mM. From these "seafloor" values, concentrations decrease by an average 0.69 mM/m, again with variance according to stations and transect (Tr1 = -0.58 mM/m, Tr2 = -0.57 mM/m, Tr3 = -1.09 mM/m; and Tr4 = -0.60 mM/m). The dissolved S gradients across all stations within SNESS range from -0.41 to -1.13 mM/m. Total dissolved S at the Lomonosov Ridge station displays a significantly steeper decrease than any other station (-1.92 mM/m). Importantly, decreases in dissolved S are similar in magnitude to increases in alkalinity at each station examined. Indeed, the molar ratio of alkalinity change to sulfur change ($-\Delta Alkalinity/\Delta S$) is 0.98 (Fig. 9a).

4.4 Ammonia and phosphate

The C:N:P molar ratio of typical marine organic matter is approximately 106:16:1 (Redfield, 1958; Takahashi, 1985). Although this ratio differs for terrestrial organic carbon (closer to 134:9:1, Tian et al., 2010), dissolved HPO_4^{2-} and NH_4^+ concentrations in pore water can be used in a general sense to assess consumption of particulate organic carbon. This is because the degradation releases these species to pore water (Froelich et al., 1979). Notably, concentrations of NH_4^+ and HPO_4^{2-} are near or below detection in samples immediately below the seafloor (Fig. 4-8).

Dissolved NH_4^+ profiles increase almost linearly with depth, although with slight concave-down curvature. Similar to alkalinity profiles, NH_4^+ concentrations rise with depth below the seafloor more at stations with shallower water depth (although we note an exception for Tr2). Across stations along the four transects, pore water NH_4^+ concentrations increase with depth on average by 38.69 μM/m, with a range from 11.3 to 76.1 μM/m. Along each transect, the average

408 NH_4^+ gradients are as follows: Tr1 = 43.0 μM/m, Tr2 = 17.4 μM/m, Tr3 = 69.0 μM/m, and Tr4 =
409 29.0 μM/m.

410 By contrast, concentrations of dissolved HPO_4^{2-} in our cores typically increase to a
411 subsurface maximum, and then decrease (Fig. 4-8). Based on the available data, a more
412 pronounced maximum appears to occur at stations with relatively shallow water depth. For
413 example, consider the peak in HPO_4^{2-} concentrations at four stations. At the two shallow stations,
414 S12 (384 m) and S22 (367 m) the HPO_4^{2-} maxima are, 73 μM (1.91 m) and 18 μM (0.66 m),
415 respectively, but at the two deeper stations, S17 (977 m) and S14 (733 m), the HPO_4^{2-} maxima
416 are only 6.7 μM (1.76 m) and 7.1 μM (2.33 m) respectively. The station on Lomonosov Ridge
417 (S31) has a high in HPO_4^{2-} concentration of 76 μM at 1.02 m below the seafloor. In general,
418 stations with more pronounced HPO_4^{2-} maxima also have greater increases in alkalinity with
419 depth.

420 The NH_4^+, HPO_4^{2-}, and alkalinity profiles relate to one another statistically, although with
421 some distinctions. All stations have a C:N ratio in pore waters much higher than the canonical
422 Redfield Ratio of 6.625 (Fig. 10). Rather, the concentration relationship of alkalinity and
423 ammonium ion can be expressed by a second order polynomial ($[NH_4^+] = -0.003[Alk]^2 + 0.105$
424 $[Alk] – 0.253$; Fig. 9b) with an average molar ratio (Alk/NH_4^+) of 14.7, close to that expected for
425 degradation of terrestrial organic carbon. Interestingly, this ratio deviates somewhat across
426 transects, increasing at sites from Tr1, Tr3, Tr2, to the Lomonosov Ridge station. Across all
427 stations and above the subseafloor HPO_4^{2-} peak, the molar ratio of alkalinity to phosphate ion
428 (Alk/HPO_4^{2-}) averages 55.7 in pore water samples. This ratio also generally increases in cores
429 from east to west.
430

4.5 Metals

At most stations, dissolved Ba^{2+} concentrations increase nonlinearly from values at or below detection limit (0.01 μM) near the seafloor to generally constant values (0.6 – 0.7 μM) within 0.8 m below the seafloor. However, at several stations, dissolved Ba^{2+} concentrations remain at or below the detection limit for all samples.

Overall, dissolved Ca^{2+}, Mg^{2+}, and Sr^{2+} concentrations decrease with depth (Fig. 4-8). For the stations along the four transects, Ca^{2+} concentrations drop on average between -0.09 and -0.12 mM/m (Tr1), about -0.09 mM/m (Tr2), between -0.09 and -0.10 (Tr3), and -0.075 mM/m (Tr4). Magnesium concentrations also drop, the average change being between -0.43 and -0.48 mM/m (Tr1), between -0.27 and -1.32 (Tr2), between -0.86 and -0.94 mM/m (Tr3), and -0.467 mM/m (Tr4). Strontium concentrations decrease an average of 0.3 μM/m, considering all stations along the four transects (Tr1 = 0.5 μM/m, Tr2 = 0.3 μM/m, Tr3 = 0.1 μM/m, and Tr4 = 0.1 μM/m). The station on Lomonosov Ridge again stands apart. At this location, the decreases in dissolved Ca^{2+}, Mg^{2+}, and Sr^{2+} are 0.27 mM/m, 1.24 mM/m, and 0.50 μM/m, respectively.

The profiles of dissolved Mn and Fe are complicated in terms of location. Generally, profiles show a broad rise in concentrations within the upper sediment and a subsequent drop in concentrations at deeper depth. Some stations have a maxima in dissolved Mn (Stations S12 (135 μM at 5 m), S28 (66 μM at 3.1 m), and Lomonosov Ridge (86 μM at 1.3 m), where concentrations decrease below. At other stations, however, Mn concentrations still appear to be increasing at the lowest depth. Iron concentrations are generally below the detection limit at or near the seafloor, and begin increasing around 2.5 – 3.5 m, reaching concentrations upward of 20 μM.

5. Discussion

5.1 Fidelity of rhizon pore water measurements

Researchers have employed multiple methods to extract pore waters from marine sediments over the last few decades, but the rhizon technique remains relatively novel (e.g., Seeberg-Elverfeldt et al., 2005; Dickens et al., 2007; Pohlman et al., 2008). Several studies have questioned the accuracy and precision of analyses obtained through this approach (e.g., Schrum et al., 2012; Miller et al., 2014). Two experiments conducted during the SWERUS-C3 Leg 2 Expedition using the Rhizons suggest that part of the problem concerns the timing and location of sampling (Supplementary Information). Notably, however, as clearly documented in previous works (Seeberg-Elverfeldt et al., 2005; Dickens et al., 2007; Pohlman et al., 2008), rhizon sampling can lead to "smooth" concentration profiles for multiple dissolved species, including alkalinity (Fig. 4-8).

Concerns about rhizon sampling may be valid for dissolved components when concentration gradients are very low. For example, Schrum et al. (2012) stressed alkalinity differences between samples collected at similar depth using rhizon sampling and conventional squeezing. However, the total alkalinity range in this study was between 1.6 and 2.6 mM, and typical differences were 0.06 mM. A similar finding occurs in the dissolved Ca^{2+} and Ba^{2+} profiles of this study, where the range in values is small and adjacent samples deviate by more than analytical precision (Tbl. 1, Fig. S3). However, when the signal to noise ratio becomes high, as true with most dissolved components at most stations (Fig. 4-8), the rhizon sampling renders pore water profiles with well-defined concentration gradients that can be interpreted in terms of chemical reactions and fluxes.

5.2 General absence of methane

Direct measurements of dissolved CH_4 in deep-sea sediment are complicated (Claypool and Kvenvolden 1983). During core retrieval and depressurization, major CH_4 loss can occur from pore space (Dickens et al., 1997). Importantly, in sediments recovered through piston coring and where *in situ* CH_4 concentrations significantly exceed solubility conditions at 1 Atm pressure, gas release typically generates sub-horizontal cracks ("gas voids") that span the core between the liner. No such cracks were documented in any of the cores.

Excluding St31 on the Lomonosov Ridge, there is no indication of a shallow SMT in any of the cores. Interstitial water sulfur concentrations do not drop below 22.8 mM within the upper 8 m. In fact, calculated downward SO_4^{2-} fluxes, as inferred from sulfur concentration gradients (Tbl. 2) range from -1.8 to -6.2 mol/m^2-kyr for all stations except Station S31. For comparison, a site with a near seafloor temperature of 2 °C (Fig. S2) and porosities similar to those measured (Fig. S1), an SMT at 6.0 mbsf would imply a SO_4^{2-} flux of -40 mol/m^2-kyr.

Given the lack of HS^- and the measured pH (Fig. S2), alkalinity should closely approximate HCO_3^- concentrations (Eqn. 4). Estimated HCO_3^- fluxes ($JHCO_3^-$) do not exceed 6.8 mol/m^2-kyr at any station east of the Lomonosov Ridge (Tbl. 2). For comparison, at sites with abundant CH_4 at depth, $JHCO_3^-$generally exceeds 30 mol/m^2-kyr above the SMT (Tbl. 2). These extreme fluxes arise because methanogenesis in deeper sediment drives an upward flux of HCO_3^- (Fig. 3), and because AOM contributes additional HCO_3^- and HS^- to pore water at the SMT (Eqn. 1).

The δ^{13}C-DIC values of pore water decrease with depth at all stations, almost in concert with the rise in alkalinity, implying no CH_4 production because methanogenesis would increase δ^{13}C-DIC values (Fig. 9c; Whiticar, 1999). Other than Station S31, the lowest value of δ^{13}C-DIC is -25.23 ‰ at 5.5 m at Station S22 (Fig. 6). This is interesting because a series of microbial

reactions utilizing POM can lead to higher alkalinity and lower δ^{13}C-DIC values in pore water. The most important of these reactions is organoclastic sulfate reduction (OSR), which can be expressed as (Berner, 1980; Boudreau and Westrich, 1984):

$$2CH_2O + SO_4^{2-} \rightarrow H_2S + 2HCO_3^- . \quad (7)$$

As emphasized previously, methane-charged sediment sequences do occur on continental slopes in the Arctic. Of particular interest to this study are locations in the Beaufort Sea, where indications for gas hydrate manifest on seismic profiles (Grantz et al., 1976; Grantz et al., 1982; Weaver and Stewart, 1982; Hart et al., 2011; Phrampus et al., 2014), and pore water profiles have been generated using shallow piston cores (Coffin et al., 2013). Striking contrasts exist between pore water profiles of the Beaufort Sea and those of SNESS (Tbl. 2). In the Beaufort Sea, there are moderate to high downward SO_4^{2-} and upward CH_4 fluxes (1.9 to 154.8 mol/m^2-kyr), shallow SMTs (6.29 to 1.06 mbsf), high DIC fluxes between the SMT and the mudline (46.3 to 242.6), and negative δ^{13}C-DIC values at SMT's (≈ -20‰).

5.3 Special case: Lomonosov Ridge station

Station 31 on the Lomonosov Ridge (Fig. 8) differs from all other stations examined in this study. Here, pore water chemistry profiles hint at CH_4 in pore space within shallow sediment. Extrapolation of the dissolved S profile suggests an SMT at approximately 14 mbsf. This depth lies within the range common for locations with AOM (D'Hondt et al., 2002), notably including well studied sites on Blake Ridge (Borowski et al., 1999). Similar to some sites with CH_4, the δ^{13}C-DIC values become very "light"; indeed, the value at the base of the core, -43.5‰, almost necessitates CH_4 oxidation within shallow sediment. Comparably steep alkalinity (1.6 mM/m) and NH_4 gradients (60.4 μM/m) also characterize most sites with CH_4 near the seafloor.

However, there is an issue concerning reduced sulfur, which is a product of AOM (Eqn. 1). If AOM was occurring at ~13.9 mbsf, one might expect evidence for HS^- migrating from below (Fig. 3). No ZnS precipitated in pore waters of this core upon addition of ZnAc.

A comparison of published DIC fluxes, SO_4^{2-} fluxes, and SMT depths (Tbl. 2) reveals fluxes decrease exponentially with SMT depth (Fig. 11). In fact, a fundamental relationship exists when one considers that upward CH_4 fluxes control the SMT depth (Eqn. 1; Fig. 3). The modest SO_4^{2-} flux (-13.9 mol/m^2-kyr) and alkalinity flux (11.3 mol/m^2-kyr) estimated for the Lomonosov Ridge station conform to those expected for an SMT at about 14 mbsf. For example, Hensen et al. (2003) calculated a SO_4^{2-} flux of -14.7 mol/m^2-kyr for a site with an SMT at 14 mbsf in the Argentine Basin, and Berg (2008) calculated a SO_4^{2-} flux of -8.05 mol/m^2-kyr for a site with an SMT at 16 mbsf along the Costa Rica Margin.

5.4 Other chemistry

Microbial communities preferentially utilize the most energetically favorable oxidant available leading to a characteristic reaction sequence in marine sediment (Froelich et al., 1979; Berner, 1980; D'Hondt et al., 2004). With increasing depth below the seafloor, these include: aerobic respiration, denitrification, manganese oxide reduction, iron oxide reduction, SO_4^{2-} reduction, and finally methanogenesis. Many of the cores collected across SNESS appear to terminate in the zone of metal oxide reduction. This is because, at most stations, Mn and Fe profiles are still increasing at the bottom of the sampled interval (Fig. 4-8), presumably due to dissimilatory Mn- and Fe-oxide reduction. However, Mn may be more complicated. März et al., (2011) find evidence from Mn profiles along the southern Mendeleev Ridge that suggest diagenetic remobilization of Mn at depth and diffusion toward shallow sediments. The relatively

546 deep depths of metal oxide reduction nevertheless, are consistent with a relatively low input of
547 POM to the seafloor, and completely contrast with most sites where high CH_4 concentrations
548 exist in shallow sediment. A simple interpretation is that there is insufficient input of POC over
549 time to drive methanogenesis near the seafloor.

550 The station on the Lomonosov Ridge again stands apart. Here, Mn and Fe concentrations
551 reach maxima at 1.3 mbsf and 0.5 mbsf, respectively, and decrease below. This is likely due to
552 Mn and Fe produced during dissimilatory oxide reduction, but where both metals precipitate
553 below into carbonate (Mn and Fe) or sulfide phases (Fe; Jørgensen et al., 1990; März et al.,
554 2011). This is common at locations with modest POC input, and the Lomonosov Ridge site
555 appears to receive higher organic carbon burial over time than all the other locations examined.
556 Given the relationship of alkalinity to ammonia (Fig. 10), much of the organic matter on the
557 continental slope may derive from terrestrial rather than marine sources (Müller and Suess, 1979;
558 Reimers et al., 1992), but a more detailed study of sedimentation rates and organic matter content
559 and composition is required to elucidate these relationships further.

560

561 *5.5 Signatures of AOM and OSR*

562 Some authors have used changes in DIC and SO_4^{2-} concentrations between the seafloor and
563 the SMT to infer the relative importance of AOM and OSR in marine sediments (Kastner et al.
564 2008b; Luo et al. 2013; Hu et al. 2015). This idea can be expressed by comparing
565 $\Delta(DIC+Ca^{2+}+Mg^{2+})$ and ΔSO_4^{2-}, where Ca^{2+} and Mg^{2+} are included to account for loss of DIC
566 via carbonate precipitation (other authors, such as Snyder et al., 2007 and Wehrmann et al.,
567 (2011) use fluxes instead of concentrations). The rationale lies in the fact that the C:S ratio for
568 AOM is 1:1 (Eqn. 1), whereas the C:S ratio for OSR is 2:1 (Eqn. 7). However, this approach

neglects two considerations: (1) changes in concentration do not directly relate to fluxes, because of differences in diffusivities of various ionic species, and, (2) a flux of HCO_3^- from below the SMT can augment the DIC produced from AOM or OSR at or above the SMT (Dickens and Snyder, 2009). Thus, changes in alkalinity relative to SO_4^{2-} often exceed 1:1, even at locations completely dominated by AOM (Chatterjee et al., 2011).

Rather than comparing changes in C:S molar ratios or going through detailed flux calculations to interrogate the importance of the two reactions in shallow sediment, one might also incorporate the δ^{13}C-DIC values. This is because δ^{13}C-DIC values and the depth of DIC production differ considerably across many sites where either AOM or OSR dominates. We generate a figure expressing these relationships at multiple sites (Fig. 12), where the y-axis is:

$$\frac{\Delta(DIC + Ca^{2+} + Mg^{2+})}{\Delta(SO_4^{2-})}, \quad (8)$$

and the x-axis is: DIC*δ^{13}C-DIC. The C:S ratios of dissolved species lie above 1:1 at most locations, regardless of whether CH_4 exists in shallow sediment and AOM dominates, as highlighted by Chatterjee et al. (2011). However, sites with significant CH_4 have considerably more negative DIC*δ^{13}C-DIC values. Notably, pore waters from all stations examined here, except S31 on the Lomonosov Ridge, have modest DIC*δ^{13}C-DIC values consistent with a dominance of OSR in shallow sediment rather than AOM.

In summary, from general pore water considerations as well as from comparisons to pore water profiles at other locations, sediments across SNESS do not contain CH_4 over extensive areas of shallow sediment. Implicit in this finding is that sediment sequences in this region lack widespread gas hydrate. As models for gas hydrate occurrence in the Arctic (Fig. 1) correctly predict gas hydrate in several regions (e.g., Kvenvolden and Grantz, 1990; Max and Lowrie,

590 1993; Max and Johnson, 2012), our findings prompt an interesting question: why are predictions
591 so markedly wrong for the SNESS?
592
593 *5.6 Possible explanations for widespread absence of gas hydrate and methane*
594 To understand the likely absence of widespread gas hydrates across SNESS, one needs to
595 consider the generalities of their occurrence in marine sediment. There are two basic conditions
596 for gas hydrate on continental slopes (Kvenvolden, 1993; Dickens, 2001). The first consideration
597 is the "potential volume", or the pore space where physiochemical conditions (e.g., temperature,
598 pressure, salinity, sediment porosity) are amenable to gas hydrate formation. As stressed in
599 previous works, because of cold bottom water and a low geothermal gradient, the region has a
600 relatively large volume of sediment with appropriate gas hydrate stability conditions (Stranne et
601 al., 2016). The second consideration is the "occupancy", or the fraction of sediment pore space
602 with sufficient CH_4 to precipitate gas hydrate. While environmental conditions across SNESS are
603 highly conducive for gas hydrate formation, pore water profiles strongly indicate little to no CH_4
604 exists in the upper hundred meters of sediment.
605 This inference strongly depends on recognition as to how diffusive systems operate in
606 marine sediment. Hundreds of pore water profiles have been generated during scientific ocean
607 drilling expeditions, including scores into CH_4 charged sediment sequences. These profiles
608 almost universally show vertical connectivity of pore water chemistry over hundreds of meters
609 (Fig. 3). Moreover, away from local sites of advection, pore water profiles are generally similar
610 over extensive areas. This occurs because, given sufficient permeability and time, diffusive
611 fluxes transport species from intervals of high concentration to intervals of low concentration.
612 Hence, unless some impermeable layer exists in the sediment sequence, even CH_4 at depth

613 impacts near seafloor concentrations. Indeed, work on the outer Blake Ridge wonderfully shows
614 this phenomenon. The uppermost gas hydrate in sediment in this region lies at about 190 mbsf
615 (Borowski et al., 1999). Nonetheless, its presence occurs over ~26,000 km^2 and affects shallow
616 pore water profiles across this region, because the flux of CH_4 from depth drives AOM near the
617 seafloor (Borowski et al., 1999; Dickens, 2001).
618 No seafloor features indicative of seafloor CH_4 expulsion were found during the
619 bathymetric mapping of SNESS. Nonetheless, it is possible that local CH_4 venting, perhaps
620 related to and mediated by bubble transport, could occur away from transects and cores of
621 SWERUS Leg 2. Certainly, the chemistry of advecting fluids toward seafloor features such as
622 mud volcanoes and cold seeps typically differs from the much broader surrounding region (Luff
623 and Wallmann, 2003; Coffin et al., 2007; Hiruta et al., 2009; Hu et al., 2010; Coffin et al., 2014;
624 Hu et al., 2015). However, in such cases, even the encompassing area typically has shallow
625 SMTs. Without invoking odd geology, such as an extensive impermeable layer, it is unlikely that
626 significant CH_4 exists in shallow sediment across much of SNESS, including as gas hydrate or
627 free gas. Here it is stressed that neither gas hydrate nor free gas can exist in sediment on
628 continental slopes without high concentrations of dissolved gas in surrounding pore water
629 (Dickens et al., 1997; Hiruta et al., 2009; Geprägs et al., 2016). The surprising lack of CH_4 across
630 SNESS, as inferred from pore water profiles, suggests insufficient *net* input of POC over time, so
631 that either methanogenesis has not occurred or the product has been lost.
632 The accumulation of POC within the SNESS region may be relatively low over the Plio-
633 Pleistocene. With low POC inputs, other microbial reactions can exhaust the labile organic
634 matter needed for methanogenesis. This may, in fact, explain why the pore water chemistry
635 suggests that metal-oxide reduction dominates the geochemical environment at most of our

636 stations. Without further investigation, we offer four possibilities (not mutually exclusive) as to
637 why this might occur: (1) significant sea-ice concentrations, both at present-day and during past
638 glacial intervals, greatly diminishes primary production of marine organic carbon within the
639 water column; (2) the extremely broad continental shelf prevents large accumulations of
640 terrestrial organic rich sediment from reaching the slope; (3) highly variable sediment
641 accumulation, perhaps corresponding to glacial-interglacial oscillations, creates a situation where
642 POC from either source is consumed during time intervals of low deposition; and although not
643 directly related to POC accumulation (4) changes in sea level during the last glacial maximum
644 caused much of the hydrate to outgas as the stability zone moved downslope (Stranne et al.,
645 2016). With the third explanation, large land-based glaciers in the past may have physically
646 scoured sediment (and organic matter) from the upper slope (Jakobsson et al., 2014).
647 Importantly, the first three explanations distinguish the SNESS region from the Beaufort Sea,
648 where abundant CH_4 in shallow sediment unquestionably occurs (Coffin et al., 2011, Treude et
649 al., 2014).
650 In earlier times, particularly the Cretaceous through Early Eocene (Jenkyns et al., 2004;
651 Sluijs et al., 2006; Backman et al., 2009), organic-rich sediment may have accumulated at high
652 rates throughout the Arctic. Definitely on Lomonosov Ridge in the central Arctic, Lower Eocene
653 sediments contain high organic carbon and potential indicators of past methanogenesis (e.g.,
654 barium mobilization). As these cores contain no CH_4 at present day, presumably if CH_4 was
655 generated, it has been lost in the intervening time. Should these organic-rich horizons be buried
656 across the SNESS region and presently generating CH_4 via thermogenesis, the gas is too deeply
657 buried to affect shallow sediment.
658

6. Conclusions

Leg 2 of the SWERUS-C3 expedition recovered sediments and pore waters from numerous stations across the continental slopes North of the East Siberian Sea (SNESS). These stations extend from Wrangel Island to the New Siberian Islands, and provide information from a climatically sensitive but highly inaccessible area.

In an effort to understand CH_4 cycling within the SNESS region, we generated detailed pore water profiles of multiple dissolved constituents. The pore water profiles are coherent and interpretable, and give a general view: most stations have low SO_4^{2-} and HCO_3^- fluxes (<6.2 and 6.8 mol/m^2-kyr respectively), a moderate decrease in δ^{13}C-DIC values with depth (-3.6‰/m average), no dissolved H_2S, moderate rise in HPO_4^{2-} and NH_4 concentrations, and slightly decreasing Ca^{2+}, Mg^{2+}, and Sr^{2+} concentrations. Except for one station on the Lomonosov Ridge, metal oxide reduction appears to be the dominant geochemical environment affecting shallow sediment, and there is no evidence for upward diffusing CH_4. These results strongly suggest that gas hydrates do not occur on any of our depth transects spread across the continental slope in this region of the Arctic Ocean. This directly conflicts with ideas in multiple publications, which generally have assumed large quantities of CH_4 and gas hydrate. However, it remains possible that significant CH_4 occurs where the Lomonosov Ridge intersects the continental margin as well as westward on the Laptev Sea continental slope.

Acknowledgments. The authors would like to thank the SWERUS-C3 Leg 2 crew as well as reviewers.

Table List

Table 1 - QA/QC

Table 2 - Published and Calculated Fluxes

a = Coffin et al., 2013; b = Personal Communication; c = Coffin et al., 2007; d = Coffin et al., 2006; e = Coffin et al., 2008; f = Hamdan et al., 2011 and Coffin et al., 2014; g = Dickens and Snyder, 2009; h= Snyder et al., 2007; i = Mountain et al., 1994; j = Lin et al., 2006; k = Berelson et al., 2005; l = Hensen et al., 2003; m = Dickens, 2001; n = Geprags et al., 2016; o = Claypool et al., 2006; p = Keigwin et al., 1998; q = Berg, 2008; r = Borowski et al., 2000; s = D'Hondt et al., 2002; t = D'Hondt et al., 2004; u = Torres et al., 2009; v = Burns, 1998; w = Kastner et al., 2008; x = Paull et al., 1996; y = Flood et al., 1995; z = Wefer et al., 1998; 1 = Prell et al., 1998; 2 = Takahashi et al., 2011; 3 = Riedel et al., 2006; 4 = Tamaki et al., 1990; 5 = Lyle et al., 1997; 6 = Moore et al., 2001; 7 = Kimura et al., 1997; 8 = Suess et al., 1988; 9 = D'Hondt et al., 2003. ‡ = Calculated from published material.

Figure Captions

Figure 1. Generalized Arctic map with background from GeoMapApp (http://www.geomapapp.org; Ryan et al., 2009). Observed sulfate-methane transitions during the MITAS 1 expedition shown in black diamonds (Coffin et al., 2013) and Arctic Coring Expedition (ACEX) shown as red squares (Backman et al., 2009).

Figure 2. Bathymetric map of Eurasian Arctic showing the overall cruise track of Leg 2 along with the four transects and coring locations. Multicores shown as yellow triangles, gravity and piston cores as white stars, and the ship trackline as gray line from Barrow, Alaska.

Figure 3. Idealized pore water concentration profiles for high and low upward methane flux. Discrete data points for sites 722 (Arabian Sea; Seifert and Michaelis, 1991; D'Hondt et al., 2002) and 1230 (offshore Peru; Donohue et al., 2006) are given as reference.

Figure 4. Transect 1. results. IAPSO standard seawater (black dotted line) shown for comparison.

712

713 **Figure 5.** Transect 2. results. IAPSO standard seawater (black dotted line) shown for
714 comparison.
715

716 **Figure 6.** Transect 3. results. IAPSO standard seawater (black dotted line) shown for
717 comparison.
718

719 **Figure 7.** Transect 4. results. IAPSO standard seawater (black dotted line) shown for
720 comparison.
721

722 **Figure 8.** Lomonosov Ridge Station results. IAPSO standard seawater (black dotted line), and
723 representative stations from the four transects shown for comparison.
724

725 **Figure 9.** Relationship of (a) sulfate change (ΔSO_4^{2-}) and carbonate corrected alkalinity change
726 ($\Delta Alk+Ca^{2+}+Mg^{2+}$); (b) the second order polynomial association of NH_4^+ to Alkalinity; and (c)
727 decreasing δ^{13}C-DIC values with alkalinity increase. Methane charged sites (1230, 1426, and
728 1427; 1230, Shipboard Scientific Party, 2003; 1426 and 1427, Expedition Scientists, 2014) given
729 for comparison.
730

731 **Figure 10.** C:N:P ratio indirectly shown with $\Delta Alk/\Delta NH_4^+$ and $\Delta Alk/\Delta HPO_4^{2-}$. Several global
732 sites, 994, 995, 997, 1059, 1225, 1230, 1426, 1427, and 1319 (994-997, 1059, Borowski et al.,
733 2000; 1225 and 1230, Shipboard Scientific Party, 2003; 1426 and 1427, Expedition Scientists,
734 2014) given for comparison. Blue marginal distribution curves show global distribution while
735 red gives SNESS stations (this project). SNESS pore waters have higher C:N and lower C:P than
736 comparative sites.
737

738 **Figure 11.** Bicarbonate (HCO_3^-) and sulfate (SO_4^{2-}) flux exponential relationship with SMT
739 depth for all sites listed in Tbl. 2.
740

741 **Figure 12.** Ratio of carbonate corrected alkalinity change ($\Delta Alk+Ca^{2+}+Mg^{2+}$) and sulfate change
742 (ΔSO_4^{2-}) to the product of DIC and δ^{13}C-DIC value (AT13-2 and KC151, Kastner et al., 2008a;

PC02-PC14, Coffin et al., 2008; 994-997, 1059, Borowski et al., 2000; Paull et al., 2000; 1326 and 1329, Torres and Kastner, 2009; GC233 and GB425, Hu et al., 2010; D-5 – D-8 and D-F, Hu et al., 2015; C9-C19, Luo et al., 2013; PC-07, Smith and Coffin, 2014; 1230, Shipboard Scientific Party, 2003; 1244 and 1247, Claypool et al., 2006; 1305 and 1306, Party, 2005) including global sites for comparison) showing the paucity of methane charged sites actually reaching 1:1 C:S ratio. Error bars are one sigma. SNESS plotted pore waters substitute alkalinity for DIC. With the absence of sulfide, DIC and alkalinity should be roughly equivalent in these pore waters. SNESS locations use the same symbols as previous figures.

751 **References:**

752 Aagaard, K., Coachman, L. K., and Carmack, E. C.: On the halocline of the Arctic Ocean, Deep
753 Sea Res., 28, 529-545, 1981.

754 Aagaard, K. and Carmack, E. C.: The role of sea ice and other fresh water in the Arctic
755 Circulation, J. Geophys. Res., 94, 14485–14498, 1989.

756 Aharon, P. and Fu, B.: Microbial sulfate reduction rates and sulfur and oxygen isotope
757 fractionations at oil and gas seeps in deepwater Gulf of Mexico. Geochimica et
758 Cosmochimica Acta, 64(2), pp.233-246, 2000.

759 Alekseev, M. N.: Paleogeography and geochronology in the Russian eastern arctic during the
760 second half of the quaternary, Quatern. Int., 41/42, 11–15, 1997.

761 Alperin, M. J., Reeburgh, W. S., and Whiticar, M. J.: Carbon and hydrogen isotope fractionation
762 resulting from anaerobic methane oxidation, Global Biogeochem. Cy., 2, 279-288, 1988.

763 Archer, D.: A model of the methane cycle, permafrost, and hydrology of the Siberian continental
764 margin, Biogeosciences, 12 (10), 2953–2974, 2015.

765 Augstein, E.: Die Expedition ARCTIC'96 mit FS" Polarstern"(ARK XII) mit der Arctic Climate
766 System Study (ACSYS); The expedition ARCTIC'96 of RV" Polarstern"(ARK XII) with
767 the Arctic Climate System Study (ACSYS). Berichte zur Polarforschung (Reports on
768 Polar Research), 234, 1997.

769 Backman, J., and Moran, K.: Expanding the Cenozoic paleoceanographic record in the Central
770 Arctic Ocean: IODP Expedition 302 Synthesis: Central European Journal of Geosciences,
771 1, 2, 157-175, 2009.

772 Bakhmutov, V., Whitledge, T., Wood, K. and Ostrovskiy, A.: Report on the execution of marine
773 research in the Bering Strait, East Siberian and the Chukchi Sea by the Russian-American

774 Expedition under the program of" RUSALCA" during the period from 23 August through
775 30 September, 2009.
776 Barnes, R. O. and Goldberg, E. D.: Methane production and consumption in anoxic marine
777 sediments, Geol. 4, 297–300, 1976.
778 Beaudoin, Y. C., Waite, W., Boswell, R., and Dallimore, S. R.: Frozen Heat: A UNEP Global
779 Outlook on Methane Gas Hydrates. Volume 1. UN. Environ. Programme, GRID-Arendal,
780 2014.
781 Berelson, W. M., Prokopenko, M., Sansone, F. J., Graham, A. W., McManus, J. and Bernhard, J.
782 M.: Anaerobic diagenesis of silica and carbon in continental margin sediments: discrete
783 zones of TCO 2 production. Geochimica et cosmochimica acta, 69 (19), 4611-4629,
784 2005.
785 Berg, P., Risgaard-Petersen, N., and Rysgaard, S.: Interpretation of measured concentration
786 profiles in sediment pore water, Limnol. Oceanogr., 43, 1500-1510, 1998.
787 Berg, R.D.: Diffusional methane fluxes within continental margin sediments and depositional
788 constraints on formation factor estimates, ProQuest, 2008.
789 Berner, R. A.: Diagenetic models of dissolved species in the interstitial waters of compacting
790 sediments, Am. J. Sci., 275, 88–96, 1975.
791 Berner, R. A.: Stoichiometric models for nutrient regeneration m anoxic sediment?, Limnology,
792 22, 781-786, 1977.
793 Berner, R. A.: Early Diagenesis: A Theoretical Approach, Princeton University Press, Princeton,
794 N. J., 1980.

795 Bhatnagar, G., Chatterjee, S., Chapman, W. G., Dugan, B., Dickens, G. R., and Hirasaki G. J.:
796 Analytical theory relating the depth of the sulfate-methane transition to gas hydrate
797 distribution and saturation, Geochem. Geophy. Geosy., 12, 1-21, 2011.
798 Biastoch, A., Treude, T., Ruepke, L. H., Riebesell, U., Roth, C., Burwicz, E. B., Park, W., Latif,
799 M., Boening, C. W., Madec, G., and Wallmann, K.: Rising Arctic Ocean temperatures
800 cause gas hydrate destabilization and ocean acidification, Geophys. Res. Lett., 38, 1-5,
801 2011.
802 Boetius, A., Ravenschlag, K., Schubert, C. J., Rickert, D., Widdel, F., Gieseke, A., Amann, R.,
803 Jørgensen, B. B., Witte, U. and Pfannkuche, O.: A marine microbial consortium
804 apparently mediating anaerobic oxidation of methane, Nature, 407, 623-626, 2000.
805 Borowski, W. S., Paull, C. K., and Ussler III, W.: Marine porewater sulfate profiles indicate in
806 situ methane flux from underlying gas hydrate, Geol. 24, 655– 658, 1996.
807 Borowski, W. S., Paull, C. K., and Ussler W. III: Global and local variations of interstitial sulfate
808 gradients in deepwater, continental margin sediments: Sensitivity to underlying methane
809 and gas hydrates, Mar. Geol., 159, 131–154, 1999.
810 Borowski, W. S., Hoehler, T. M., Alperin, M. J., Rodriguez, N. M. and Paull, C.K.: Significance
811 of anaerobic methane oxidation in methane-rich sediments overlying the Blake Ridge gas
812 hydrates. In Proceedings of the ocean drilling program, scientific results (Vol. 164, pp.
813 87-99, 2000).
814 Borowski, W. S., Cagatay, N., Ternois, Y., and Paull, C. K.: Data Report: carbon isotopic
815 composition of dissolved CO2, CO2 gas, and methane, Blake –Bahama Ridge and
816 Northeast Bermuda Rise, ODP Leg 172, In: Keigwin, L. D., Rio, D., Acton, G. D.,

817 Arnold, E. (Eds.), Proceedings of the ODP. Scientific Results (College Station, TX), vol.
818 172, 1–16, 2001.
819 Boudreau, B. P. and Westrich, J. T.: The dependence of bacterial sulfate reduction on sulfate
820 concentration in marine sediments, Geochimica Cosmochimica Acta, 48, 2503–2516,
821 1984.
822 Buffett, B. and Archer, D.: Global inventory of methane clathrate: sensitivity to changes in the
823 deep ocean, Earth Planet. Sc. Lett., 227, 185–199, 2004.
824 Burns, S.J.: Carbon isotopic evidence for coupled sulfate reduction-methane oxidation in
825 Amazon Fan sediments. Geochimica et Cosmochimica Acta, 62(5), 797-804, 1998.
826 Carcione, J. M. and Tinivella, U.: Bottom-simulation reflectors: Seismic velocities and AVO
827 effects, Geophysics, 65, 54–67, 2000.
828 Chatterjee, S., Dickens, G. R., Bhatnagar, G., Chapman, W. G., Dugan, B., Snyder, G. T., and
829 Hirasaki, G. J.: Pore water sulfate, alkalinity, and carbon isotope profiles in shallow
830 sediment above marine gas hydrate systems: A numerical modeling perspective, J.
831 Geophys. Res-Sol. Ea., 116, 1-25, 2011.
832 Claypool, G. E. and Kvenvolden, K. A.: Methane and other hydrocarbon gases in marine
833 sediment, Annu. Rev. Earth Pl. Sc., 11, 299-327, 1983.
834 Claypool, G. E., Milkov, A. V., Lee, Y. J., Torres, M. E., Borowski, W.S., and Tomaru, H.:
835 Microbial Methane Generation and Gas Transport in Shallow Sediments of an
836 Accretionary Complex, Southern Hydrate Ridge (ODP Leg 204), Offshore Oregon USA,
837 In: Trehu, A.M., Bohrmann, G., Torres, M.E., Colwell, F.S. (Eds.), In Proceedings of the
838 ODP, Scientific Results. Ocean Drilling Program, College Station, Texas, 2006.

839 Cline, J. D.: Spectrophotometric determination of hydrogen sulfide in natural waters, Limnol.
840 Oceanogr., 14, 454-458, 1969.
841 Coffin, R. B., Pohlman, J. W., Gardner, J., Downer, R., Wood, W., Hamdan, L., Walker, S.,
842 Plummer, R., Gettrust, J., and Diaz, J.: Methane hydrate exploration on the mid Chilean
843 coast: a geochemical and geophysical survey, J. Petrol. Sci. Eng., 56, 32-41, 2007.
844 Coffin, R., Hamdan, L., Pohlman, J., Wood, W., Pecher, I., Henrys, S., Greinert, J., and Faure,
845 K.: Geochemical characterization of concentrated gas hydrate deposits on the Hikurangi
846 Margin, New Zealand. Preliminary Geochemical Cruise Report. NRL/MR/ 6110-07,
847 2007.
848 Coffin, R. B., Hamdan, L. J., Plummer, R., Smith, J., Gardner, J., Hagen, R., and Wood, W.:
849 Analysis of Methane and Sulfate Flux in Methane-charged Sediments from the
850 Mississippi Canyon, Gulf of Mexico, Mar. Petrol. Geol., 25, 977–987, 2008.
851 Coffin, R. B., Plummer, R. B., Yoza, B., Larsen, R. K., Millholland, L. C., and Montgomery, M.
852 T.: Spatial variation in shallow sediment methane sources and cycling on the Alaskan
853 Beaufort Sea Shelf/Slope, Mar. Petrol. Geol., 45, 186-197, 2013.
854 Coffin, R. B., Hamdan, L. J., Smith, J. P., Rose, P. S., Plummer, R. E., Yoza, B., Pecher, I. and
855 Montgomery, M.T.: Contribution of vertical methane flux to shallow sediment carbon
856 pools across Porangahau ridge, New Zealand. Energies, 7 (8), 5332-5356, 2014.
857 Collett, T. S., Lee, M. W., Agena, W. F., Miller, J. J., Lewis, K. A., Zyrianova, M. V., Boswell,
858 R., and Inks, T. L.: Permafrost associated natural gas hydrate occurrences on the Alaska
859 North Slope, Mar. Petrol. Geol., 28, 279-294, 2010.
860 D'Hondt, S., Rutherford, S., and Spivack, A.J.: Metabolic activity of subsurface life in deep-sea
861 sediments, Science, 295, 2067-2070, 2002.

D'Hondt, S. L., Jørgensen, B. B., Miller, D. J., and Shipboard Scientific Pary: Proceedings of the Ocean Drilling Program, Initial Reports Volume 201, 2003.

D'Hondt, S., Jørgensen, B. B., Miller, D. J., Batzke, A., Blake, R., Cragg, B. A., Cypionka, H., Dickens, G. R., Ferdelman, T., Hinrichs, K. U. and Holm, N.G.: Distributions of microbial activities in deep subseafloor sediments. Science, 306 (5705), 2216-2221, 2004.

Danyushevskaya, A., Yashin, D. S., and Kirillow, O. V.: Geochemical patterns of distribution of organic carbon in the bottom sediments of Arctic seas, Oceanology, 20, 183-188, 1980.

Darby, D. A., Naidu, A. S., Mowatt, T. C., and Jones, G.: Sediment composition and sedimentary processes in the Arctic Ocean. In: Y. Herman (Editor), The Arctic Seas: Climatology, Oceanography, Geology and Biology, Van Nostrand Reinhold, New York, 657-720, 1989.

Dickens, G. R., Paull, C. K. and Wallace, P.: Direct measurement of in situ methane quantities in a large gas hydrate reservoir. Nature, 385, 426-428, 1997.

Dickens, G. R.: Sulfate profiles and barium fronts in sediment on the Blake Ridge. Present and past methane fluxes through a large gas hydrate reservoir, Geochim. Cosmochim. Ac., 65, 529-543, 2001.

Dickens, G. R.: Rethinking the global carbon cycle with a large, dynamic and microbially mediated gas hydrate capacitor. EPSL, 213 (3), 169-183, 2003.

Dickens, G. R.: Rhizon sampling of pore waters on scientific drilling expeditions: an example from the IODP Expedition 302, Arctic Coring Expedition (ACEX). Sci. Drill 4, 22–25, 2007.

884 Dickens, G.R. and Snyder, G.T.: Interpreting upward methane flux from marine pore water
885 profiles, In: Fire in the Ice, NETL Methane Hydrate Newsletter 9 (1), 7-10, 2009.
886 D'Hondt, S., Rutherford, S., and Spivack, A. J.: Metabolic activity of subsurface life in deep-sea
887 sediments, Science, 295, 2067–2070, 2002.
888 Dmitrenko, I. A., Polyakov, I. V., Kirillov, S. A., Timokhov, L. A., Frolov, I. E., Sokolov, V. T.,
889 Simmons, H. L., Ivanov, V. V., and Walsh, D.: Toward a warmer Arctic Ocean:
890 spreading of the early 21st century Atlantic Water warm anomaly along the Eurasian
891 Basin margins, J. Geophys. Res-Oceans 113, 1-13, 2008.
892 Dmitrenko, I. A., Bauch, D., Kirillov, S. A., Koldunov, N., Minnett, P. J., Ivanov, V. V.,
893 Hölemann, J. A., and Timokhov, L. A.: Barents Sea upstream events impact the
894 properties of Atlantic water inflow into the Arctic Ocean: Evidence from 2005 to 2006
895 downstream observations, Deep-Sea Research I, 56, 513–527, 2009.
896 Donohue, C. M., Snyder, G. T., and Dickens, G. R.: Data report: major cation concentrations of
897 interstitial waters collected from deep sediments of Eastern Equatorial Pacific and Peru
898 Margin (ODP Leg 201), Proceedings of ODP, Scientific Results, 201, Ocean Drilling
899 Program, College Station, TX, 2006.
900 Dymond, J., Suess, E., and Lyle, M.: Barium in deep-sea sediment: A geochemical proxy for
901 paleoproductivity, Paleoceanography 7, 163–181, 1992.
902 Elliott, S., Maltrud, M., Reagan, M., Moridis, G., and Cameron-Smith P.: Marine methane cycle
903 simulations for the period of early global warming, J. Geophys. Res-Biogeo., 116, 1-13,
904 2011.
905 Engen, Ø., Faleide, J. I., and Dyreng, T. K.: Opening of the Fram Strait gateway: A review of
906 plate tectonic constraints: Tectonophysics, 450, 1-69, 2008.

907 Expedition 346 Scientists: Asian Monsoon: onset and evolution of millennial-scale variability of
908 Asian monsoon and its possible relation with Himalaya and Tibetan Plateau uplift, IODP
909 Preliminary Report, 346, 2014.
910 Ferré, B., Mienert, J., and Feseker, T.: Ocean temperature variability for the past 60 years on the
911 Norwegian-Svalbard margin influences gas hydrate stability on human time scales, J.
912 Geophys. Res., 117, 1-14, 2012.
913 Flood, R. D., Piper, D. J. W., Klaus, A., and Scientific Research Party: Proceedings of the Ocean
914 Drilling Program, Initial Reports, 155: College Station, TX (Ocean Drilling Program),
915 1995.
916 Froelich, P., Klinkhammer, G. P., Bender, M. A. A., Luedtke, N. A., Heath, G. R., Cullen, D.,
917 Dauphin, P., Hammond, D., Hartman, B., and Maynard, V.: Early oxidation of organic
918 matter in pelagic sediments of the eastern equatorial Atlantic: suboxic diagenesis,
919 Geochim. Cosmochim. Ac., 43, 1075-1090, 1979.
920 Geprägs, P., Torres, M. E., Mau, S., Kasten, S., Römer, M., and Bohrmann, G.: Carbon cycling
921 fed by methane seepage at the shallow Cumberland Bay, South Georgia, sub-Antarctic,
922 Geochem. Geophy. Geosy., 17, 1401-1418, 2016.
923 Gieskes, J. M. and Rogers, W. C.: Alkalinity determination in interstitial waters of marine
924 sediments, J. Sediment. Res., 43(1), 272-277, 1973.
925 Gieskes, J. M., Gamo, T., and Brumsack, H.: Chemical methods for interstitial water analysis
926 aboard JOIDES Resolution, 1991.
927 Gingele, F. and Dahmke, A.: Discrete barite particles and barium as tracers of paleoproductivity
928 in South Atlantic sediments, Paleoceanography, 9, 151–168, 1994.

929 Giustiniani, M., Tinivella, U., Jakobosson, M., and Rebesco, M.: Arctic Ocean gas hydrate
930 stability in a changing climate, J. Geol. Res., 1-10, 2013.
931 Goldhaber, M.: Kinetic Models of Sulfur Diagenesis in Recent Marine Sediments, In
932 Transactions-AGU, 55, 696-697, 1974.
933 Grantz, A., Boucher, G., and Whitney, O. T.: Possible solid gas hydrate and natural gas deposits
934 beneath the continental slope of the Beaufort Sea, U.S. Geological Survey Circulation
935 Number 733, 1976.
936 Grantz, A., Mann, D. M., and May, S. D.: Tracklines of multichannel seismic-reflection data
937 collected by the U.S. Geological Survey in the Beaufort and Chukchi Seas in 1977 for
938 which profiles and stack tapes are available, U.S. Geological Survey Open-File Report
939 1982, 82-735, 1982.
940 Greinert, J., Bohrmann, G., and Suess, E.: Gas hydrate-associated carbonates and methane-
941 venting at Hydrate Ridge: classification, distribution, and origin of authigenic lithologies,
942 Natural gas hydrates: Occurrence, distribution, and detection, 99-113, 2001.
943 Haacke, R. R., Westbrook, G. K., and Riley, M.: Controls on the formation and stability of gas
944 hydrate-related bottom-simulating reflectors (BSRs): a case study from the west Svalbard
945 continental slope, J. Geophys. Res., 113, 1-17, 2008.
946 Hamdan, L. J., Gillevet, P. M., Pohlman, J. W., Sikaroodi, M., Greinert, J., and Coffin, R.B.:
947 Diversity and biogeochemical structuring of bacterial communities across the Porangahau
948 ridge accretionary prism, New Zealand, FEMS Microbiol. Ecol., 77, 518-532, 2011.
949 Haraldsson, C., Anderson, L. G., Hassellöv, M., Hulth, S., and Olsson, K.: Rapid, high-precision
950 potentiometric titration of alkalinity in ocean and sediment pore waters, Deep Sea
951 Research Part I: Oceanographic Research Papers, 44, 2031-2044, 1997.

952 Hart, P. E., Pohlman, J. W., Lorenson, T. D., and Edwards, B. D.: Beaufort Sea Deep-water gas
953 hydrate recovery from a seafloor mound in a region of widespread BSR occurrence, in
954 Proceedings of the 7th International Conference on Gas Hydrates (ICGH 2011),
955 Edinburgh, Scotland, 2011.
956 Hensen, C., Zabel, M., Pfiefer, K., Schwenk, T., Kasten, S., Riedinger, N., Schulz, H. D.,
957 Boetius, A.: Control of sulfate porewater profiles by sedimentary events and the
958 significance of anaerobic oxidation of methane for the burial of sulfur in marine
959 sediments, Geochimica Cosmochimica Acta 67, 2631-2647, 2003.
960 Hiruta, A., Snyder, G.T., Tomaru, H. and Matsumoto, R., 2009. Geochemical constraints for the
961 formation and dissociation of gas hydrate in an area of high methane flux, eastern margin
962 of the Japan Sea. Earth and Planetary Science Letters, 279(3), pp.326-339.
963 Holbrook, W. S., Hoskins, H., Wood, W. T., Stephen, R. A., and Lizarralde, D.: Methane hydrate
964 and free gas on the Blake ridge from vertical seismic profiling, Science, 273, 1840–1843,
965 1996.
966 Holmes, R. M., McClelland, J. W., Peterson, B. J., Shiklomanov, I. A., Shiklomanov, A. I.,
967 Zhulidov, A. V., Gordeev, V. V., and Bobrovitskaya, N. N.: A circumpolar perspective
968 on fluvial sediment flux to the Arctic Ocean, Global Biogeochem. Cy., 16, 1-14, 2002.
969 Holler, T., Wegener, G., Knittel, K., Boetius, A., Brunner, B., Kuypers, M. M., and Widdel, F.:
970 Substantial 13C/12C and D/H fractionation during anaerobic oxidation of methane by
971 marine consortia enriched in vitro, Environ. Microbiol. Rep., 1, 370-376, 2009.
972 Hu, X., Cai, W. -J, Wang, Y., Luo, S., and Guo X.: Pore-water geochemistry of two contrasting
973 brine-charged seep stations in the northern Gulf of Mexico continental slope, Mar.
974 Geochem., 118, 99–107, 2010.

975 Hu, Y., Feng, D., Liang, Q., Xia, Z., Chen, L., and Chen, D.: Impact of anaerobic oxidation of
976 methane on the geochemical cycle of redox-sensitive elements at cold-seep stations of the
977 northern South China Sea. Deep Sea Research Part II: Topical Studies in Oceanography,
978 2015.
979 Hustoft, S., Bünz, S., Mienert, J., and Chand, S.: Gas hydrate reservoir and active methane-
980 venting province in sediments on <20Ma young oceanic crust in the Fram Strait, offshore
981 NW-Svalbard, Earth Planet. Sc. Lett., 284, 12-24, 2009.
982 Hyndman, R. D. and Dallimore, S. R.: Natural gas hydrates studies, Canada Recorder, 26, 11–20,
983 2001.
984 Jakobsson, M.: Hypsometry and volume of the Arctic Ocean and its constituent seas:
985 Geochemistry, Geophysics, Geosystems, 3, 5, 1-18, 2002.
986 Jakobsson, M., Backman, J., Rudels, B., Nycander, J., Frank, M., Mayer, L., Jokat, W.,
987 Sangiorgi, F., O'Regan, M., Brinkhuis, H., King, J., and Moran, K.: The early Miocene
988 Onset of a Ventilated Circulation Regime in the Arctic Ocean: Nature, 447, 21, 986-990,
989 2007.
990 Jakobsson, M., Mayer, L., Coakley, B., Dowdeswell, J. A., Forbes, S., Fridman, B., Hodnesdal,
991 H., Noormets, R., Pedersen, R., Rebesco, M., Schenke, H. W., Zarayskaya, Y.,
992 Accettella, D., Armstrong, A., Anderson, R. M., Bienhoff, P., Camerlenghi, A., Church,
993 I., Edwards, M., Gardner, J. V., Hall, J. K., Hell, B., Hestvik, O., Kristoffersen, Y.,
994 Marcussen, C., Mohammad, R., Mosher, D., Nghiem, S. V., Pedrosa, M. T., Travaglini,
995 P. G., and Weatherall, P.: The International Bathymetric Chart of the Arctic Ocean
996 (IBCAO) Version 3.0: Geophysical Research Letters, v. 39, no. 12, p. L12609, 2012.

997 Jakobsson, M., Andreassen, K., Bjarnadóttir, L. R., Dove, D., Dowdeswell, J. A., England, J. H.,
998 Funder, S., Hogan, K., Ingólfsson, Ó., Jennings, A., Krog-Larsen, N., Kirchner, N.,
999 Landvik, J. Y., Mayer, L., Möller, P., Niessen, F., Nilsson, J., O'Regan, M., Polyak, L.,
1000 Nørgaard-Pedersen, N., and Stein, R.: Arctic Ocean glacial history, Quaternary Sci. Rev.,
1001 92, 40-67, 2014.
1002 Jørgensen, B. B., Bang, M., and Blackburn, T. H.: Anaerobic mineralization in marine sediments
1003 from the Baltic Sea-North Sea transition, Mar. Ecol. Progress Series, 59, 39-54, 1990.
1004 Jørgensen, B. B., Weber, A. and Zopfi, J.: Sulfate reduction and anaerobic methane oxidation in
1005 Black Sea sediments. Deep Sea Research Part I: Oceanographic Research Papers, 48 (9),
1006 2097-2120, 2001.
1007 Jørgensen, B. B., Böttcher, M. E., Lüschen, H., Neretin, L. N., and Volkov, I. I.: Anaerobic
1008 methane oxidation and the deep H2S sink generate isotopically heavy sulfides in Black
1009 Sea sediments, Geochim. Cosmochim. Ac., 68, 2095–2118, 2004.
1010 Jørgensen, B. B. and Parkes, R. J.: Role of sulfate reduction and methane production by organic
1011 carbon degradation in eutrophic fjord sediments (Limfjorden, Denmark), Limnol.
1012 Oceanogr, 55, 1338-1352, 2010.
1013 Jokat, W.: The expedition of the Research Vessel" Polarstern" to the Arctic in 2009 (ARK-
1014 XXIV/3). Berichte zur Polar-und Meeresforschung (Reports on Polar and Marine
1015 Research), 615, 2010.
1016 Jokat, W. and Ickrath, M.: Structure of ridges and basins off East Siberia along 81° N, Arctic
1017 Ocean, Mar. Petrol. Geol., 64, 222-232, 2015.

1018 Joye, S. B., Boetius, A., Orcutt, B. N., Montoya, J. P., Schulz, H. N., Erickson, M. J. and Lugo,
1019 S.K.: The anaerobic oxidation of methane and sulfate reduction in sediments from Gulf
1020 of Mexico cold seeps. Chemical Geology, 205 (3), 219-238, 2004.
1021 Jenkyns, H. C., Forster, A., Schouten, S., and Sinninghe Damsté, J. S.: High temperatures in the
1022 Late Cretaceous Arctic Ocean, Nature, 432, 888–892, 2004.
1023 Kastner, M., Claypool, G., and Robertson, G.: Geochemical constraints on the origin of the pore
1024 fluids and gas hydrate distribution at Atwater Valley and Keathley Canyon, northern Gulf
1025 of Mexico, Mar. Petr. Geol., 25, 860–872, 2008a.
1026 Kastner, M., Torres, M., Solomon, E., and Spivack, A. J.: Marine pore fluid profiles of dissolved
1027 sulfate; do they reflect in situ methane fluxes?, In: Fire in the Ice, NETL Methane
1028 Hydrate Newsletter, Summer, 2008b.
1029 Keigwin, L. D., Rio, D., Acton, G. D., and Shipboard Scientific Party: Proceedings of the Ocean
1030 Drilling Program, Initial Reports, 172: College Station, TX (Ocean Drilling Program),
1031 1998.
1032 Kimura, G., Silver, E. A., Blum, P., Shipboard Scientific Party: Proceedings of the Ocean
1033 Drilling Program, Initial Reports, Vol. 170, 1997.
1034 Klauda, J. B. and Sandler, S. I.: Global distribution of methane hydrate in ocean sediment,
1035 Energy Fuel, 19, 469–78, 2005.
1036 Klump, J. V. and Martens, C. S.: Biogeochemical cycling in an organic rich coastal marine
1037 basin—II. Nutrient sediment-water exchange processes, Geochim. Cosmochim. Ac., 45,
1038 101-121, 1981.

1039 Kvenvolden, K. A., and Grantz, A.: Gas hydrates in the Arctic Ocean region, in The Arctic
1040 Ocean Region, Geology of North America, Geol. Soc. of Am., Boulder, Colo., 539-549,
1041 1990.
1042 Kvenvolden, K. A.: Gas hydrates: Geological perspective and global change, Rev. Geophys., 31,
1043 173–187, 1993.
1044 Kvenvolden, K. A. and Lorenson, T. D.: The global occurrence of natural gas hydrate. In: Paull,
1045 C. K., Dillon, W. P. (Eds.), Natural Gas Hydrates: Occurrence, Distribution, and
1046 Detection, AGU Geophy. Monograph Ser., 124, 3–18, 2001.
1047 Laberg, J. S. and Andreassen, K.: Gas hydrate and free gas indications within the Cenozoic
1048 succession of the Bojornya Basin, western Barents Sea, Mar. Petrol. Geol., 13, 921-940,
1049 1996.
1050 Laberg, J. S., Andreassen, K., and Knutsen, S. M.: Inferred gas hydrate on the Barents Sea shelf
1051 a model for its formation and a volume estimate, Geo-Mar. Lett., 18, 26–33, 1998.
1052 Lerman, A.: Migrational processes and chemical reactions in Sulfate profiles and barium fronts
1053 in sediment 539 interstitial waters, In The Sea, Volume VI (ed. E. D. Goldberg), Wiley,
1054 New York, 695-738, 1977.
1055 Li, Y-H. and Gregory, S.: Diffusion of ions in sea sediments. Geochim. Cosmochim. Ac., 38,
1056 703-714, 1974.
1057 Lin, S., Hsieh, W. C., Lim, Y. C., Yang, T. F., Liu, C. S., and Wang, Y.: Methane migration and
1058 its influence on sulfate reduction in the Good Weather Ridge region, South China Sea
1059 continental margin sediments, Terr. Atmos. Ocean. Sci., 17, 883-902, 2006.
1060 Lorenson, T. D. and Kvenvolden, K. A.: Methane in coastal seawater, sea ice, and bottom
1061 sediments, Beaufort Sea, Alaska, USGS Open-File Report 95–70, 1995.

1062 Luff, R. and Wallmann, K.: Fluid flow, methane fluxes, carbonate precipitation and
1063 biogeochemical turnover in gas hydrate-bearing sediments at hydrate ridge, Cascadia
1064 margin: numerical modeling and mass balances, Geochim. Cosmochim. Ac., 67, 3403–
1065 3421, 2003.
1066 Luo, M., Chen, L., Wang, S., Yan, W., Wang, H., and Chen, D.: Pockmark activity inferred from
1067 pore water geochemistry in shallow sediments of the pockmark field in southwestern
1068 Xisha Uplift, northwestern South China Sea, Mar. Pet. Geol., 2013, 48, 247–259, 2013.
1069 Lyle, M., Koizumi, I., Richter, C., and Shipboard Scientific Party: Proceedings of the Ocean
1070 Drilling Program, Initial Reports, Vol. 167, 1997.
1071 Majorowicz, J. A. and Osadetz, K. G.: Gas hydrate distribution and volume in Canada. AAPG
1072 bulletin, 85 (7), 1211-1230, 2001.
1073 Makogon, Y. F.: Natural gas hydrates–A promising source of energy, J. Nat. Gas Sc. Eng., 2, 49-
1074 59, 2010.
1075 Malinverno, A. and Pohlman, J. W.: Modeling sulfate reduction in methane hydrate-bearing
1076 continental margin sediments: does a sulfate-methane transition require anaerobic
1077 oxidation of methane, Geochem. Geophy. Geosy., 12, 1-18, 2011.
1078 März, C., Stratmann, A., Matthiessen, J., Meinhardt, A. K., Eckert, S., Schnetger, B., Vogt, C.,
1079 Stein, R. and Brumsack, H. J.: Manganese-rich brown layers in Arctic Ocean sediments:
1080 composition, formation mechanisms, and diagenetic overprint. Geochimica et
1081 Cosmochimica Acta, 75 (23), 7668-7687, 2011.
1082 Max, M. D. and Lowrie, A.: Natural gas hydrates: Arctic and Nordic Sea potential. Arctic
1083 geology and petroleum potential, proceedings of the Norwegian Petroleum Society
1084 conference, 15-17 August 1990, Tromsø, Norway. No. 2. Elsevier Science Ltd., 1993.

1085 Max, M. D. and Johnson, A. H.: Natural Gas Hydrate (NGH) Arctic Ocean potential prospects
1086 and resource base, OTC Arctic Technology Conference, 27-53, 2012.
1087 McGuire, A. D., Anderson, L. G., Christensen, T. R., Dallimore, S., Guo, L. D., Hayes, D. J.,
1088 Heimann, M., Lorenson, D. D., MacDonald, R. W., and Roulet, N.: Sensitivity of the
1089 carbon cycle in the Arctic to climate change, Ecol. Monogr., 79, 523–555, 2009.
1090 Miles, P. R.: Potential distribution of methane hydrate beneath the European continental margins,
1091 Geophys. Res. Lett., 22, 3179-3182, 1995.
1092 Miller, M. D., Adkins, J. F., and Hodell, D. A.: Rhizon sampler alteration of deep ocean
1093 sediment interstitial water samples, as indicated by chloride concentration and oxygen
1094 and hydrogen isotopes, Geochem. Geophy. Geosy., 15, 2401-2413, 2014.
1095 Moore, G. F., Taira, A., and Klaus, A., and Shipboard Scientific Party: Proceedings of the Ocean
1096 Drilling Program, Initial Reports Volume 190, 2001.
1097 Moran, K., Backman, J., Brinkhuis, H., Clemens, S. C., Cronin, T., Dickens, G. R., Eynaud, F.,
1098 Gattacceca, J., Jakobsson, M., Jordan, R.W., and Kaminski, M.: The Cenozoic
1099 palaeoenvironment of the arctic ocean, Nature, 441, 601-605, 2006.
1100 Mountain, G. S., Miller, K. G., Blum, P., and Shipboard Scientific Party: Proc. ODP, Initial
1101 Reports, 150: College Station, TX (Ocean Drilling Program), 1994.
1102 Müller, P.J. and Suess, E., 1979. Productivity, sedimentation rate, and sedimentary organic
1103 matter in the oceans—I. Organic carbon preservation. Deep Sea Research Part A.
1104 Oceanographic Research Papers, 26(12), pp.1347-1362.
1105 Murray, R. W., Miller, D. J., and Kryc, K. A.: Analysis of major and trace elements in rocks,
1106 sediments, and interstitial waters by inductively coupled plasma–atomic emission
1107 spectrometry (ICP-AES), ODP Technical Note 29, 2000.

1108 Niewohner, C., Hensen, C., Kasten, S., Zabel, M., and Schulz, H. D.: Deep sulfate reduction
1109 completely mediated by anaerobic methane oxidation in sediments of the upwelling area
1110 off Namibia, Geochim. Cosmochim. Ac., 62, 455–464, 1998.
1111 Nöthen, K. and Kasten, S.: Reconstructing changes in seep activity by means of pore water and
1112 solid phase Sr/Ca and Mg/Ca ratios in pockmark sediments of the Northern Congo Fan,
1113 Mar. Geol., 287, 1-13, 2011.
1114 O'Regan, M., Williams, C. J., Frey, K. E., Jakobsson, M.: A synthesis of the long-term
1115 paleoclimatic evolution of the Arctic. Oceanography 24(3), 66–80, 2011.
1116 O'Regan, M., Preto, P., Stranne, C., Jakobsson, M., and Koshurnikov, A.: Surface heat flow
1117 measurements from the East Siberian continental slope and southern Lomonosov Ridge,
1118 Arctic Ocean, Geochem. Geophy. Geosy., 17, 1-15, 2016.
1119 Ostanin, I., Anka, Z., di Primio, R. and Bernal, A.: Hydrocarbon plumbing systems above the
1120 Snøhvit gas field: structural control and implications for thermogenic methane leakage in
1121 the Hammerfest Basin, SW Barents Sea. Marine and Petroleum Geology, 43, 127-146,
1122 2013.
1123 Party, S. S.: Integrated Ocean Drilling Program Expedition 303 Preliminary Report North
1124 Atlantic Climate Ice sheet–ocean atmosphere interactions on millennial timescales during
1125 the late Neogene-Quaternary using a paleointensity-assisted chronology for the North
1126 Atlantic, 1-51, 2005.
1127 Paull, C. K., Ussler, W. III, and Dillon, W. P.: Is the extent of glaciation limited by marine gas-
1128 hydrates?, Geophys. Res. Lett., 18 432–434, 1991.
1129 Paull, C. K., Matsumoto, R., Wallace, P. J., and Shipboard Scientific Party: Proceedings of the
1130 IODP, Initial Reports. Volume 164: College Station, TX, USA, 1996.

1131 Paull, C. K, Lorenson, T. D., Borowski, W. S., Ussler, III W., Olsen, K., and Rodriguez, N. M.:
1132 Isotopic composition of CH_4, CO_2 species, and sedimentary organic matter within
1133 samples from the Blake Ridge: gas source implications, In: Paull C. K., Matsumoto, R,
1134 Wallace, P. J., and Dillon, W. P., (Eds) Proceedings of the ODP, Sci. Res., Vol. 164 67–
1135 78, (ODP), 2000.
1136 Pecher, I. A., Kukowski, N., Huebscher, C., Greinert, J., and Bialas, J.: The link between bottom-
1137 simulating reflections and methane flux into the gas hydrate stability zone - new evidence
1138 from Lima Basin, Peru Margin, Earth Planet. Sc. Lett., 185, 343-354, 2001.
1139 Peterson, B. J., Holmes, R. M., McClelland, J. W., Vorosmarty, C. J., Lammers, R. B.,
1140 Shiklomanov, A. I., Shiklomanov, I. A., and Rahmstorf, S.: Increasing river discharge to
1141 the Arctic Ocean, Science, 298, 2171–2173, 2002.
1142 Phrampus, B. J., Hornbach, M. J., Ruppel, C. D., and Hart P. E.: Widespread gas hydrate
1143 instability on the upper US Beaufort margin, J. Geophys. Res-Sol. Ea., 119, 8594–8609,
1144 2014.
1145 Piñero, E., Marquardt, M., Hensen, C., Haeckel, M., and Wallmann K.: Estimation of the global
1146 inventory of methane hydrates in marine sediments using transfer functions,
1147 Biogeosciences 10, 959–975, 2013.
1148 Pohlman, J. W., Riedel, M., Waite, W., Rose, K., and Lapham, L.: Application of Rhizon
1149 samplers to obtain high-resolution pore-fluid records during geo-chemical investigations
1150 of gas hydrate systems, Fire in the Ice: Methane Hydrate Newsletter, US Department of
1151 Energy/National Energy Technology Laboratory, Fall, 2008.
1152 Polyakov, I.V., Pnyushkov, A.V. and Timokhov, L.A.: Warming of the Intermediate Atlantic
1153 Water of the Arctic Ocean in the 2000s. Journal of Climate, 25 (23), 8362-8370, 2012.

Posewang, J. and Mienert, J.: High-resolution seismic studies of gas hydrates west of Svalbard, Geo-Mar. Lett., 19, 150–156, 1999.

Prell, W. L., Niitsuma, N., and Shipboard Scientific Party: Proceedings of the Ocean Drilling Program, Initial Reports, 117: College Station, TX (Ocean Drilling Program), 1998.

Rachor, E.: The expedition ARK-XI/1 of RV" Polarstern" in 1995: [ARK XI/1, Bremerhaven-Tromsø-, 07.07. 1995-20.09. 1995]. Berichte zur Polarforschung (Reports on Polar Research), 226, 1995.

Reagan, M. T. and Moridis, G. J.: Dynamic response of oceanic hydrate deposits to ocean temperature change, J. Geophys. Res., 113, 1-21, 2008.

Reagan, M. T. and Moridis, G. J.: Large-scale simulation of methane hydrate dissociation along the West Spitsbergen margin, Geophys. Res. Lett., 36, 1-5, 2009.

Redfield, A. C.: The biological control of chemical factors in the environment, Am. Sci., 46, 221-230, 1958.

Reimers, C. E., Jahnke, R. A. and McCorkle, D. C.: Carbon fluxes and burial rates over the continental slope and rise off central California with implications for the global carbon cycle. Global Biogeochemical Cycles, 6(2), pp.199-224, 1992.

Reeburgh, W. S.: Methane consumption in Cariaco Trench waters and sediments, Earth Planet Sci. Lett., 28, 337–344, 1976.

Riedel, M., Collett, T.S., Malone, M.J., and the Expedition 311 Scientists Proceedings of the Integrated Ocean Drilling Program, Volume 311, 2006.

Riedinger, N., Kasten, S., Gröger, J., Franke, C. and Pfeifer, K.: Active and buried authigenic barite fronts in sediments from the Eastern Cape Basin, Earth Planet. Sc. Lett., 241, 876-887, 2006.

1177 Riedinger, N., Formolo, M. J., Lyons, T. W., Henkel, S., Beck, A., and Kasten, S.: An inorganic
1178 geochemical argument for coupled anaerobic oxidation of methane and iron reduction in
1179 marine sediments, Geobiology, 12, 172-181, 2014.
1180 Rudels, B., Muench, R. D., Gunn, J., Schauer, U., and Friedrich, H. J.: Evolution of the Arctic
1181 Ocean boundary current north of the Siberian shelves, Journal of Marine Systems, 25, 1,
1182 77-99, 2000.
1183 Ryan, W. B. F., Carbotte, S. M., Coplan, J. O., O'Hara, S., Melkonian, A., Arko, R., Weissel, R.
1184 A., Ferrini, V., Goodwillie, A., Nitsche, F., Bonczkowski, J., and Zemsky, R.: Global
1185 Multi-Resolution Topography synthesis, Geochem. Geophys. Geosyst., 10, 1-9, 2009.
1186 Schrum, H. S., Murray, R. S., and Gribsholt B.: Comparison of rhizon sampling and whole round
1187 squeezing for marine sediment porewater, Sci. Drill., 13, 47–50, 2012.
1188 Schulz, H. D.: Quantification of early diagenesis: dissolved constituents in marine pore water, In
1189 Mar. Geochem., Springer Berlin Heidelberg, 85-128, 2000.
1190 Seeberg-Elverfeldt, J., Schlüter, M., Feseker, T., and Kölling, M.: Rhizon sampling of pore
1191 waters near the sediment/water interface of aquatic systems, Limnol. Oceanogr. Methods,
1192 3, 361-371, 2005.
1193 Seifert, R. and Michaelis, W.: Organic compounds in sediments and pore waters of Sites 723 and
1194 724, In Prell, W.L., Niitsuma, N., et al., Proc. ODP, Sci. Results, 117: College Station,
1195 TX (ODP), 529–545, 1991.
1196 Serreze, M. C., Walsh, J. E., Chapin, III F. S., Osterkamp, T., Dyurgerov, M., Romanovsky, V.,
1197 Oechel, W. C., Morison, J., Zhang T., and Barry, R. B.: Observational evidence of recent
1198 change in the northern high-latitude environment, Climatic Change, 46, 159–207, 2000.

1199 Semiletov, I., Makshtas, O. A., Akasofu, S.I., and Andreas, E. L.: Atmospheric CO2 balance: the
1200 role of Arctic sea ice, Geophys. Res. Lett., 31, 1-4, 2004.
1201 Shakhova, N, Semiletov, I, Salyuk, A, Yusupov, V, Kosmach, D, and Gustafsson, Ö.: Extensive
1202 Methane venting to the atmosphere from sediments of the East Siberian arctic shelf,
1203 Science, 327, 1246–1250, 2010a.
1204 Shakhova, N., Semiletov, I., Leifer, I., Rekant, P., Salyuk, A., and Kosmach, D.: Geochemical
1205 and geophysical evidence of methane release from the inner East Siberian Shelf, J.
1206 Geophys. Res., 115, 1-14, 2010b.
1207 Shipboard Scientific Party: Leg 201 summary, In D'Hondt, S.L., Jørgensen, B.B., Miller, D.J., et
1208 al., Proc. ODP, Init. Repts., 201: College Station TX (Ocean Drilling Program), 1–81,
1209 2003.
1210 Sluijs, A., Schouten, S., Pagani, M., Woltering, M., Brinkhuis, H., Damsté, J.S.S., Dickens, G.R.,
1211 Huber, M., Reichart, G.J., Stein, R. and Matthiessen, J.,: Subtropical Arctic Ocean
1212 temperatures during the Palaeocene/Eocene thermal maximum. Nature, 441 (7093), 610-
1213 613, 2006.
1214 Smith, J. P. and Coffin, R. B.: Methane Flux and Authigenic Carbonate in Shallow Sediments
1215 Overlying Methane Hydrate Bearing Strata in Alaminos Canyon, Gulf of Mexico,
1216 Energies, 7, 6118-6141, 2014.
1217 Snyder, G. T., Hiruta, A., Matsumoto, R., Dickens, G. R., Tomaru, H., Takeuchi, R.,
1218 Komatsubara, J., Ishida, Y., and Yu, H.: Porewater profiles and authigenic mineralization
1219 in shallow marine sediments above the methane-charged system on Umitaka Spur, Japan
1220 Sea. Deep-Sea Research II 54, 1216–1239, 2007.

1221 Soloviev, V. A.: Gas-hydrate-prone areas of the ocean and gas-hydrate accumulations, Journal of
1222 the Conference Abstracts, 6, 158, 2002.
1223 Spencer, A. M., Embry, A.F., Gautier, D.L., Stoupakova, A.V. and Sørensen, K.: An overview of
1224 the petroleum geology of the Arctic. Geological Society, London, Memoirs, 35 (1), 1-15,
1225 2011.
1226 Spielhagen, R. F., Werner, K., Sorensen, S. A., Zamelczyk, K., Kandiano, E., Budeus, G.,
1227 Husum, K., Marchitto, T. M., and Hald, M.: Enhanced modern heat transfer to the Arctic
1228 by warm Atlantic water, Science 331, 450-453, 2011.
1229 Stein, R., Boucsein, B., and Meyer, H.: Anoxia and high primary production in the Paleogene
1230 central Arctic Ocean: First detailed records from Lomonosov Ridge, Geophys. Res. Lett.,
1231 33, 1-6, 2006.
1232 Stein, R.: Arctic Ocean sediments: processes, proxies, and paleoenvironment, Developments in
1233 Mar. Geol., 2. Elsevier, Amsterdam. 592, 2008.
1234 Stranne, C., O'Regan, M., Dickens, G. R., Crill, P., Miller, C., Preto, P., and Jakobsson, M.:
1235 Dynamic simulations of potential methane release from East Siberian continental slope
1236 sediments, Geochem. Geophy. Geosy., 17, 872-886, 2016.
1237 Stroeve, J. C., Serreze, M. C., Holland, M. M., Kay, J. E., Malanik, J., and Barrett, A. P.: The
1238 Arctic's rapidly shrinking sea ice cover: a research synthesis, Climatic Change, 110,
1239 1005-1027, 2012.
1240 Suess, E., von Huene, R., and Shipboard Scientific Party: Proceedings of the Ocean Drilling
1241 Program, Initial Reports, 112: College Station, TX (Ocean Drilling Program), 1988.
1242 Takahashi, T. Broecker, V. S., and Langer, S.: Redfield ratio based on chemical data from
1243 isopycnal surfaces, J. Geophys. Res-Oceans, 90, 6907-6924, 1985.

1244 Takahashi, K., Ravelo, A.C., Alvarez Zarikian, C.A., and the Expedition 323 Scientists
1245 Proceedings of the Integrated Ocean Drilling Program, Volume 323, 2011.
1246 Tamaki, K., Pisciotto, K., Allan, J., and Shipboard Scientific Party: Proceedings of the Ocean
1247 Drilling Program, Initial Reports, Vol. 127, 1990.
1248 Tian, H., Chen, G., Zhang, C., Melillo, J.M. and Hall, C.A.: Pattern and variation of C: N: P
1249 ratios in China's soils: a synthesis of observational data. Biogeochemistry, 98(1-3),
1250 pp.139-151, 2010.
1251 Torres, M.E., McManus, J., Hammond, D.E., De Angelis, M.A., Heeschen, K.U., Colbert, S.L.,
1252 Tryon, M.D., Brown, K.M. and Suess, E.: Fluid and chemical fluxes in and out of
1253 sediments hosting methane hydrate deposits on Hydrate Ridge, OR, I: Hydrological
1254 provinces. Earth and Planetary Science Letters, 201(3), pp.525-540, 2002.
1255 Torres, M. E., Kastner, M., Wortmann, U. G., Colwell, F., and Kim, J.: Estimates of methane
1256 production rates based on δ13C of the residual DIC in pore fluids from the Cascadia
1257 margin, EOS, 8(52), Fall Meet. Suppl., Abstract GC14A04, 2007.
1258 Torres, M. E. and Kastner M.: Data report: Clues about carbon cycling in methane-bearing
1259 sediments using stable isotopes of the dissolved inorganic carbon, IODP Expedition 311,
1260 Proceedings of the IODP, 311, 2009.
1261 Treude, T., Krause, S., Maltby, J., Dale, A.W., Coffin, R. and Hamdan, L.J.: Sulfate reduction
1262 and methane oxidation activity below the sulfate-methane transition zone in Alaskan
1263 Beaufort Sea continental margin sediments: Implications for deep sulfur cycling.
1264 Geochimica et Cosmochimica Acta, 144, 217-237, 2014.

1265 Ussler, W. and Paull, C.K.: Rates of anaerobic oxidation of methane and authigenic carbonate
1266 mineralization in methane-rich deep-sea sediments inferred from models and
1267 geochemical profiles. Earth and Planetary Science Letters, 266(3), 271-287, 2008.
1268 Wallmann, K., Pinero, E., Burwicz, E., Haeckel, M., Hensen, C., Dale, A. W., and Ruepke, L.:
1269 The global inventory of methane hydrate in marine sediments: A theoretical approach,
1270 Energies, 5, 2449–2498, 2012.
1271 Weaver, J. S. and Stewart, J. M.: In-situ hydrates under the Beaufort Sea Shelf, In: M.H. French
1272 (Editor), Proceedings of the Fourth Canadian Permafrost Conference 1981, Roger J. E.
1273 Brown Memorial Volume, Nat. Res. Council Can., Ottawa, Ont., 312-319, 1982.
1274 Wefer, G., Berger, W. H., Richter, C., and Shipboard Scientific Party: Proceedings of the Ocean
1275 Drilling Program, Initial Reports, 175: College Station, TX (Ocean Drilling Program),
1276 1998.
1277 Whiticar, M. J.: Carbon and hydrogen isotope systematics of bacterial formation and oxidation of
1278 methane. Chemical Geology, 161 (1), 291-314, 1999.
1279 Xu, D., Wu, W., Ding, S., Sun, Q. and Zhang, C.: A high-resolution dialysis technique for rapid
1280 determination of dissolved reactive phosphate and ferrous iron in pore water of
1281 sediments. Science of the total environment, 421, pp.245-252, 2012.
1282 Yamamoto, K. and Dallimore, S.: Aurora-JOGMEC-NRCan Mallik 2006–2008 Gas Hydrate
1283 Research Project progress. In: Fire in the Ice, NETL Methane Hydrate Newsletter,
1284 Summer 2008, 1–5, 2008.
1285 Ye, H., Yang, T., Zhu, G., Jiang, S., and Wu, L.: Pore water geochemistry in shallow sediments
1286 from the northeastern continental slope of the South China Sea, Mar. Petrol. Geol., 75,
1287 68-82, 2016.

Yoshinaga, M. Y., Holler, T., Goldhammer, T., Wegener, G., Pohlman, J. W., Brunner, B., Kuypers, M. M., Hinrichs, K. U. and Elvert, M.: Carbon isotope equilibration during sulphate-limited anaerobic oxidation of methane. Nature Geoscience, 7(3), 190-194, 2014.

Figures

Figure 1.

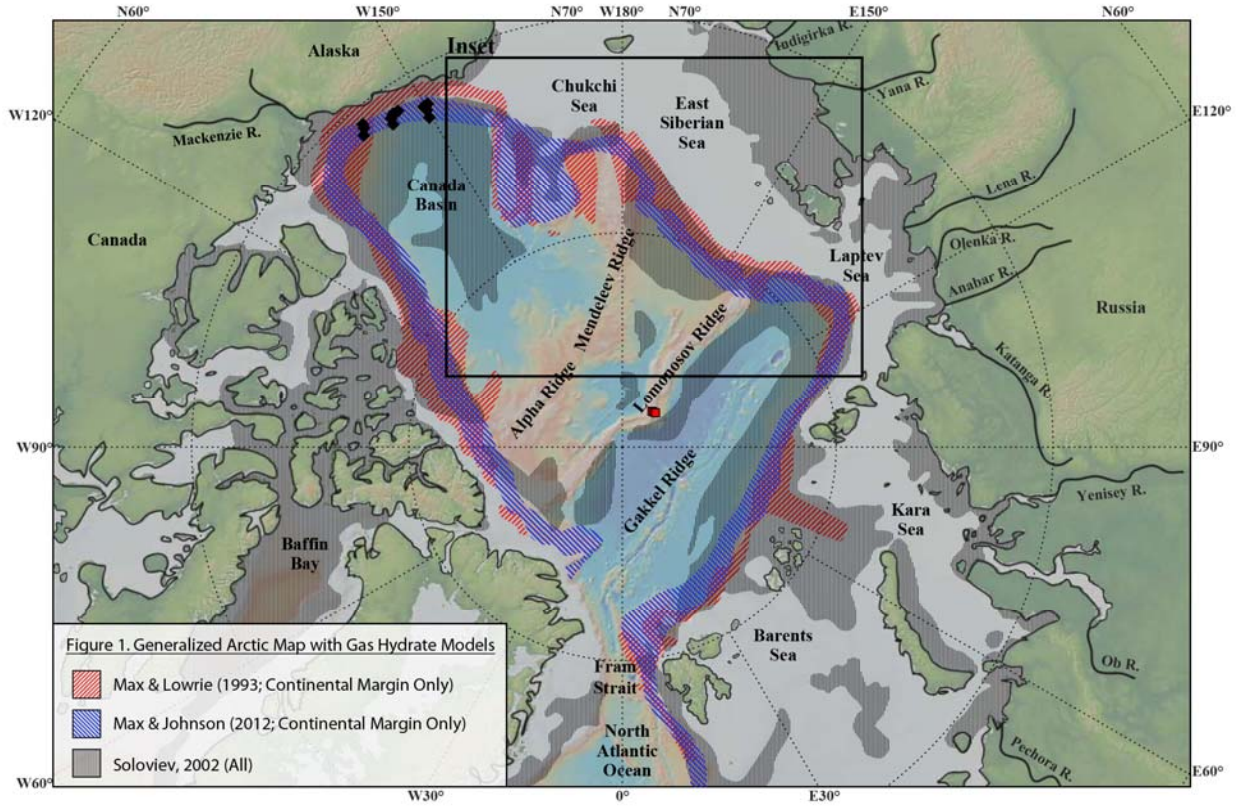

Figure 2.

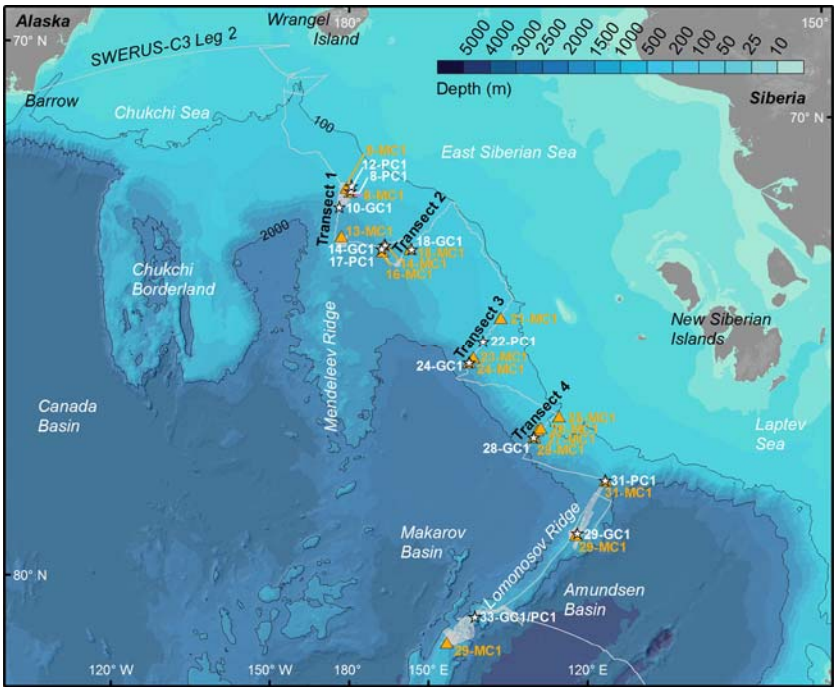
Alaska
70° N
SWERUS-C3 Leg 2
Wrangel Island
180°
150°
5000 4000 3000 2500 2000 1500 1000 500 200 100 50 25 10
Depth (m)
Barrow
Chukchi Sea
Siberia
70° N
100
East Siberian Sea
9-MC1
12-PC1
8-PC1
8-MC1
10-GC1
Transect 1
Transect 2
2000
13-MC1
14-GC1
17-PC1
18-GC1
Chukchi Borderland
16-MC1
Mendeleev Ridge
Transect 3
21-MC1
22-PC1
23-MC1
24-GC1
24-MC1
New Siberian Islands
Canada Basin
Transect 4
Laptev Sea
28-GC1
31-PC1
31-MC1
Makarov Basin
Lomonosov Ridge
29-GC1
29-MC1
80° N
Amundsen Basin
33-GC1/PC1
25-MC1
120° W
150° W
180°
150° E
120° E

Figure 3.

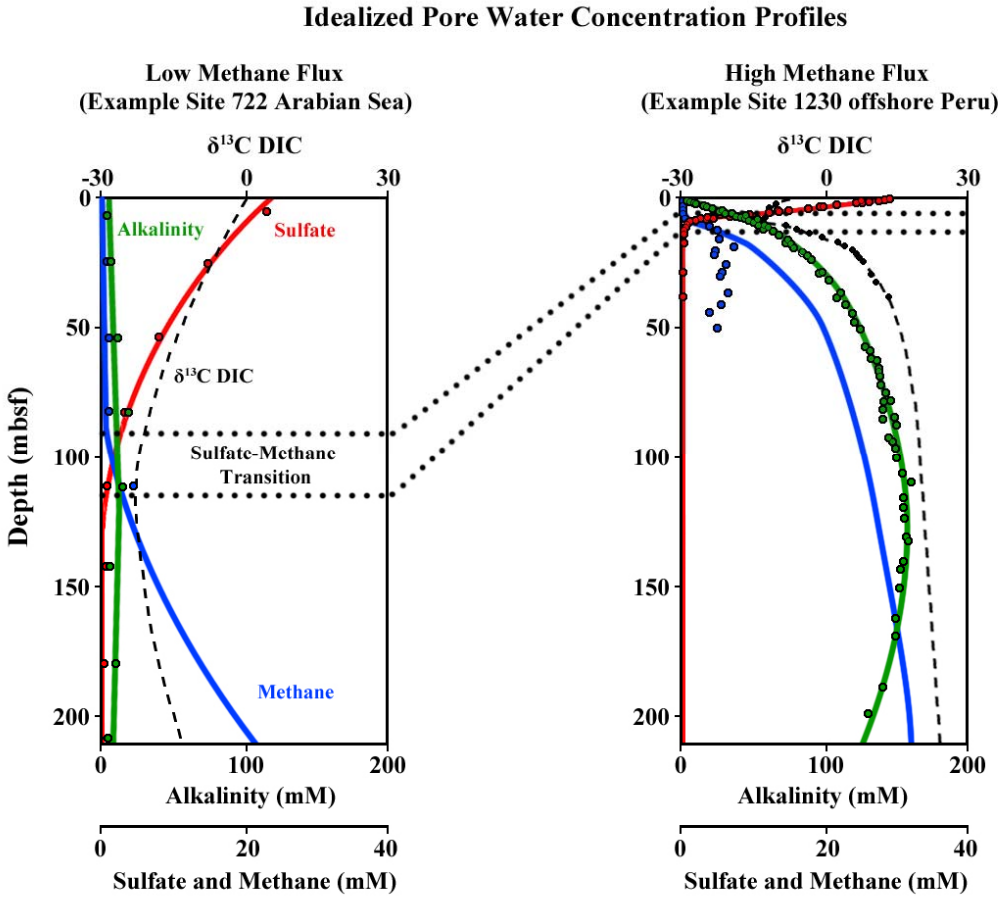
Idealized Pore Water Concentration Profiles
Low Methane Flux
(Example Site 722 Arabian Sea)
High Methane Flux
(Example Site 1230 offshore Peru)
δ13C DIC
-30
0
30
Alkalinity
Sulfate
δ13C DIC
Sulfate-Methane
Transition
Methane
Depth (mbsf)
0
50
100
150
200
Alkalinity (mM)
Sulfate and Methane (mM)
20
40

Figure 4.

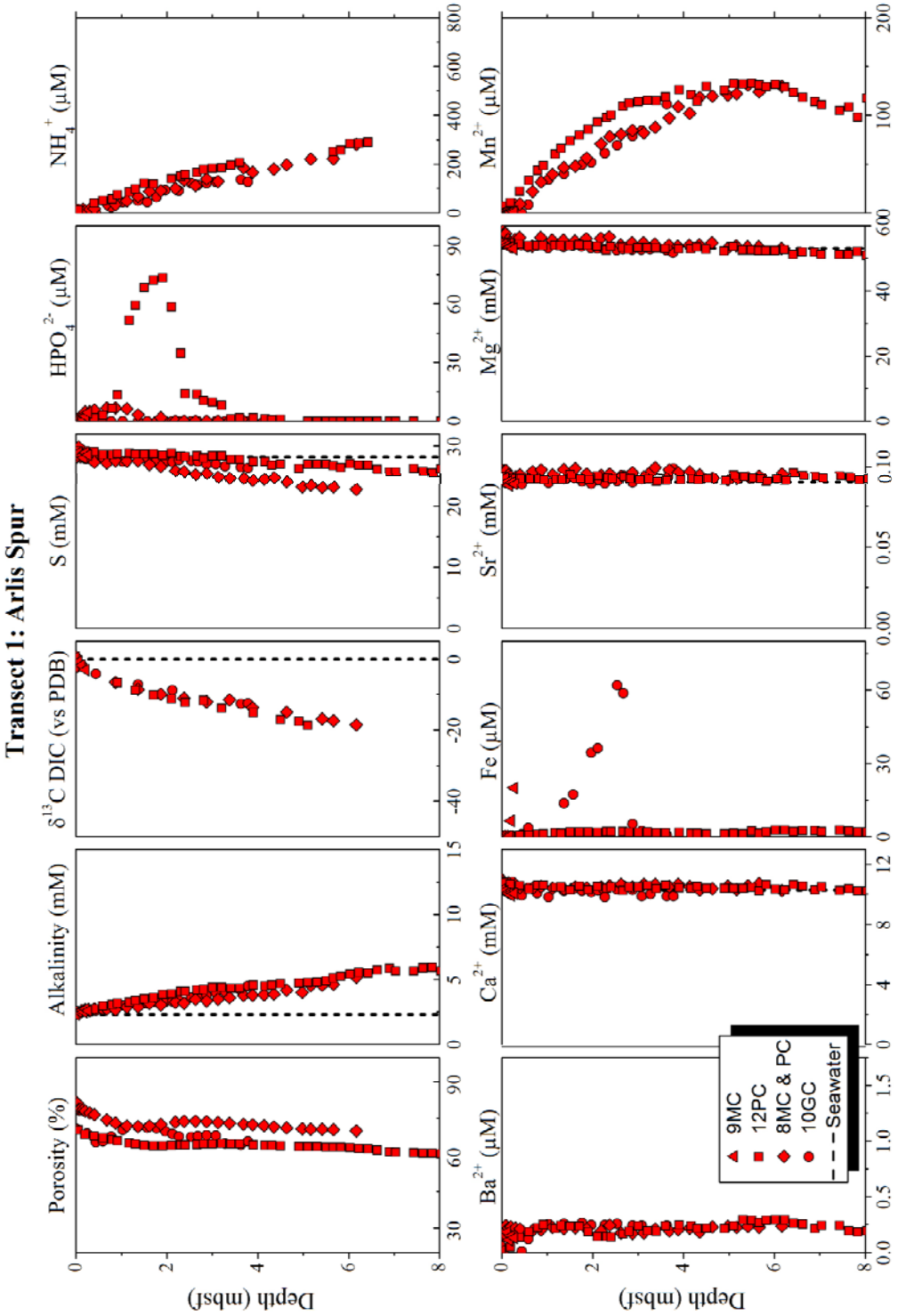
Transect 1: Arlis Spur
Porosity (%)
Alkalinity (mM)
δ13C DIC (vs PDB)
S (mM)
HPO4 2- (μM)
NH4 + (μM)
Ba2+ (μM)
Ca2+ (mM)
Fe (μM)
Sr2+ (mM)
Mg2+ (mM)
Mn2+ (μM)
Depth (mbsf)
9MC
12PC
8MC & PC
10GC
Seawater

Figure 5.

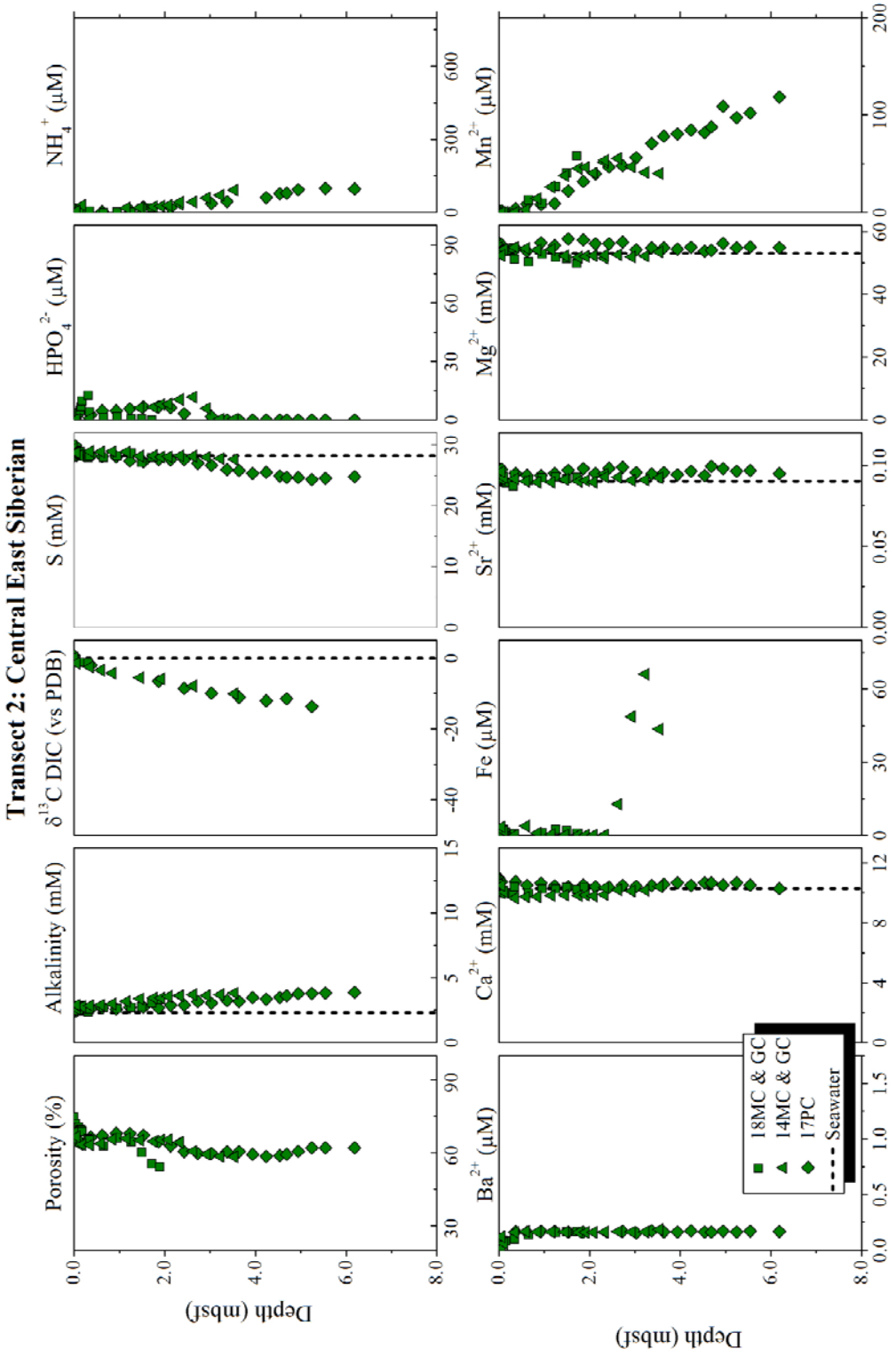
Transect 2: Central East Siberian
Porosity (%)
Alkalinity (mM)
δ13C DIC (vs PDB)
S (mM)
HPO4 2- (µM)
NH4 + (µM)
Ba2+ (µM)
Ca2+ (mM)
Fe (µM)
Sr2+ (mM)
Mg2+ (mM)
Mn2+ (µM)
18MC & GC
14MC & GC
17PC
Seawater
Depth (mbsf)
Depth (mbsf)

Figure 6.

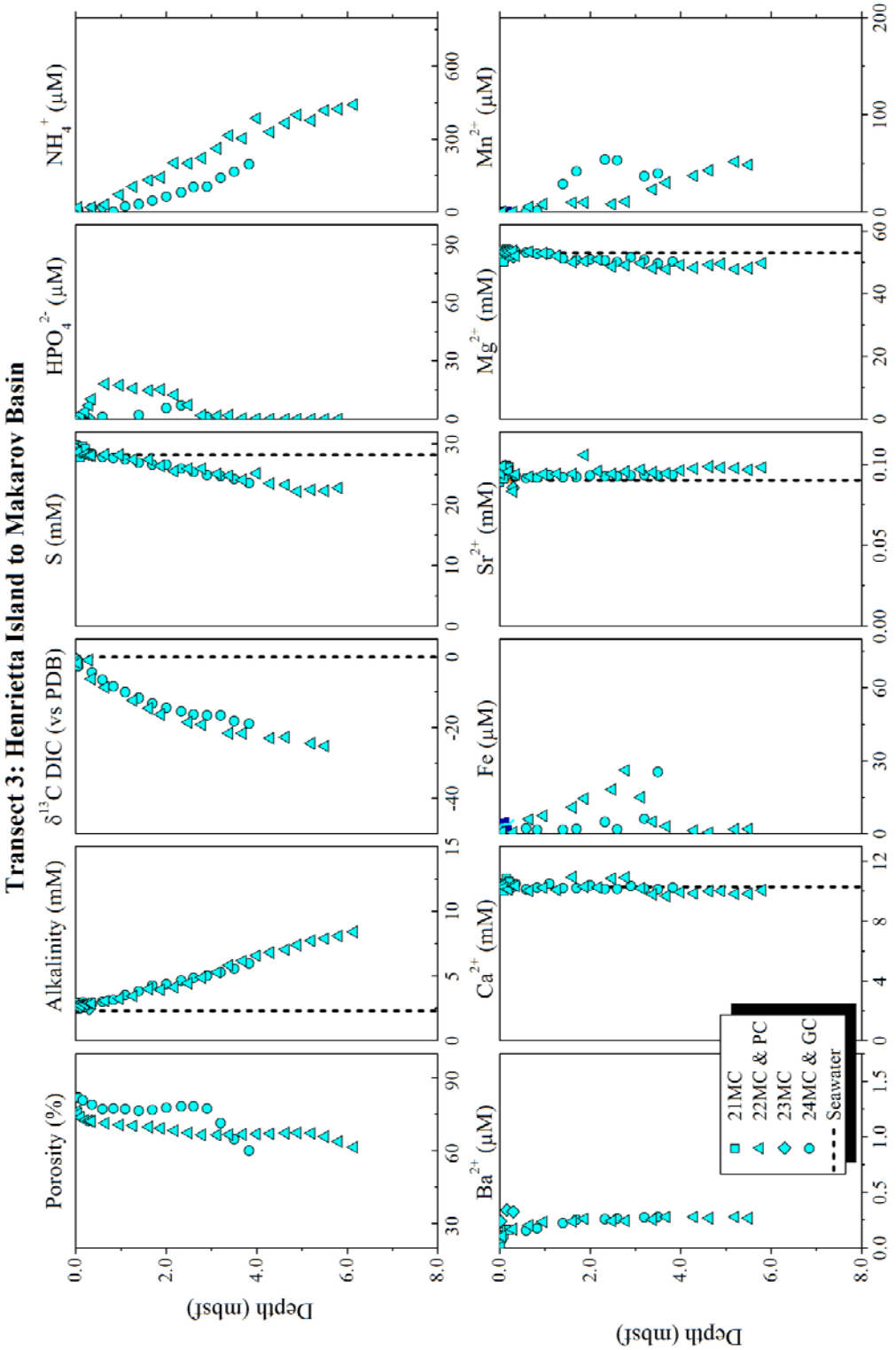
Transect 3: Henrietta Island to Makarov Basin
Porosity (%)
Alkalinity (mM)
δ^{13}C DIC (vs PDB)
S (mM)
HPO_4^{2-} (μM)
NH_4^+ (μM)
Ba^{2+} (μM)
Ca^{2+} (mM)
Fe (μM)
Sr^{2+} (mM)
Mg^{2+} (mM)
Mn^{2+} (μM)
Depth (mbsf)
21MC
22MC & PC
23MC
24MC & GC
Seawater

Figure 7.

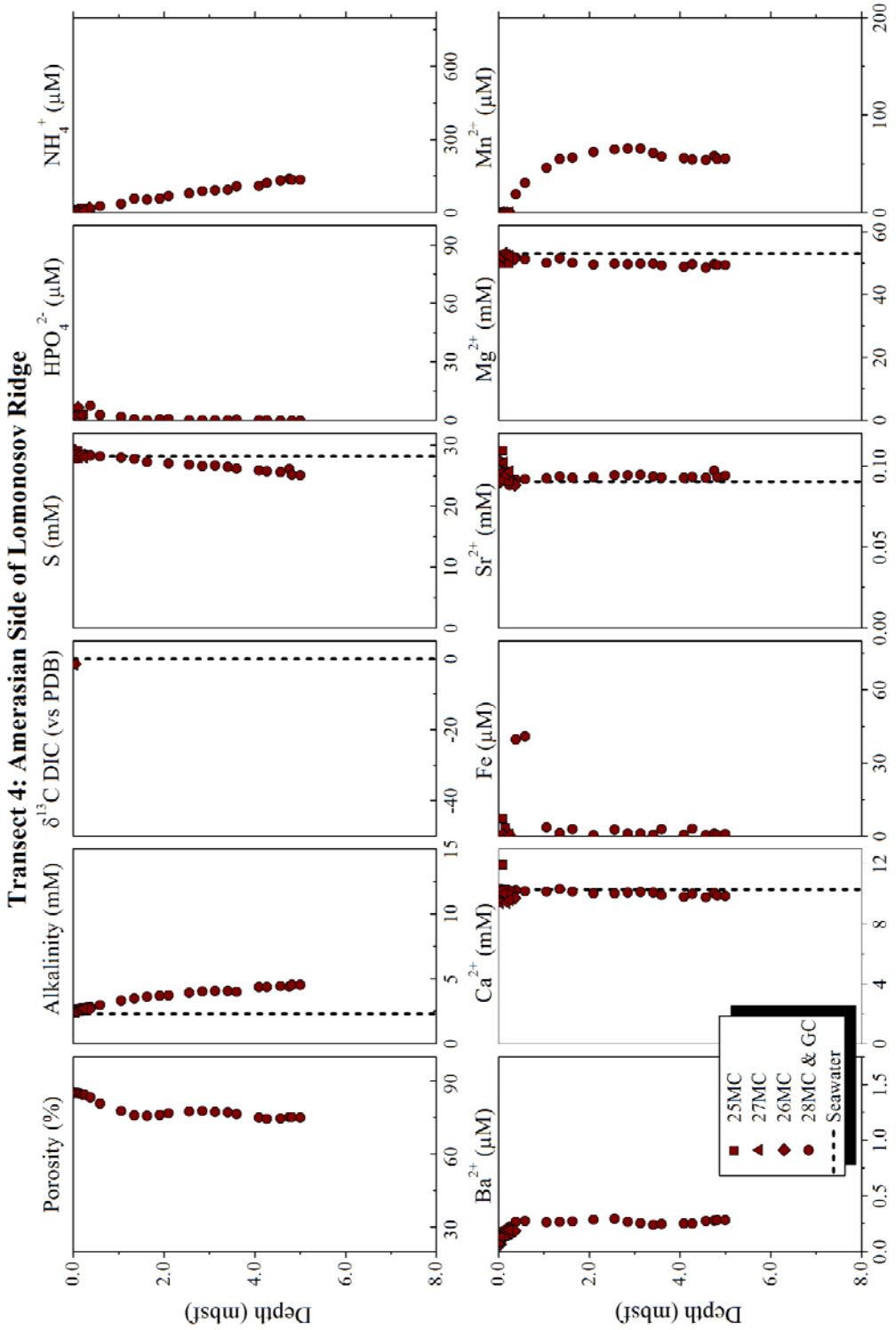
Transect 4: Amerasian Side of Lomonosov Ridge
Porosity (%)
Alkalinity (mM)
δ^{13}C DIC (vs PDB)
S (mM)
HPO_4^{2-} (μM)
NH_4^+ (μM)
Ba^{2+} (μM)
Ca^{2+} (mM)
Fe (μM)
Sr^{2+} (mM)
Mg^{2+} (mM)
Mn^{2+} (μM)
Depth (mbsf)
25MC
27MC
26MC
28MC & GC
Seawater

48 **Figure 8.**

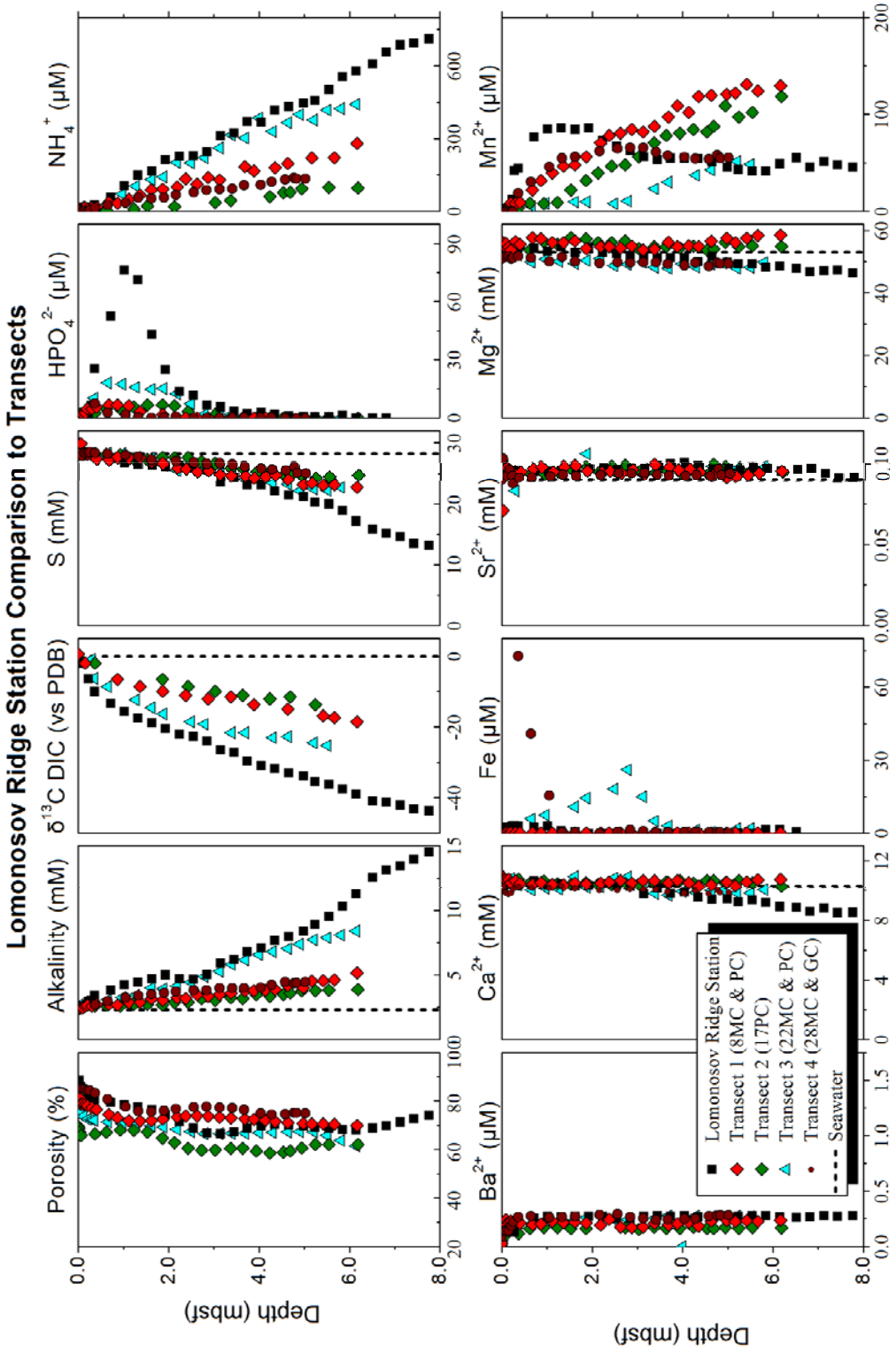

49

50

Figure 9.

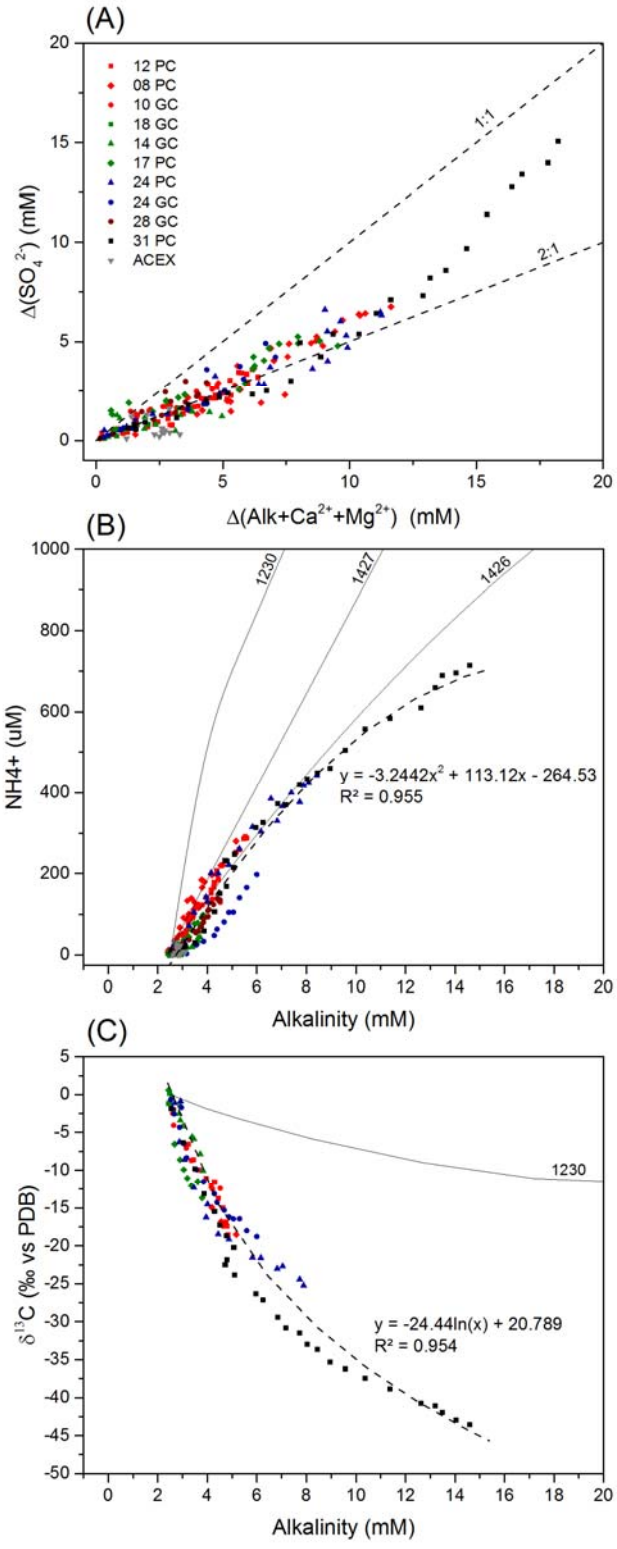
(A)
12 PC
08 PC
10 GC
18 GC
14 GC
17 PC
24 PC
24 GC
28 GC
31 PC
ACEX
1:1
2:1
Δ(SO4 2-) (mM)
Δ(Alk+Ca2++Mg2+) (mM)
(B)
1230
1427
1426
y = -3.2442x2 + 113.12x - 264.53
R² = 0.955
NH4+ (uM)
Alkalinity (mM)
(C)
1230
y = -24.44ln(x) + 20.789
R² = 0.954
δ13C (‰ vs PDB)
Alkalinity (mM)

Figure 10.

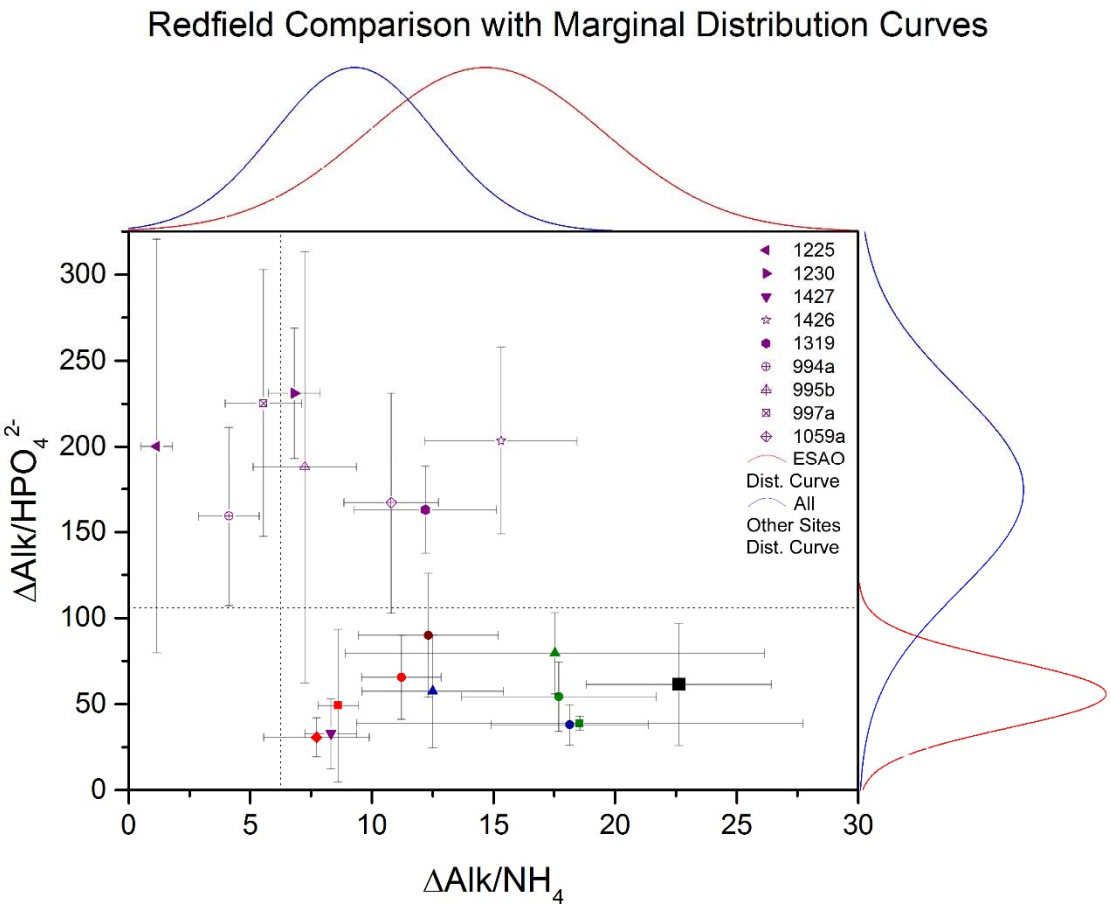
Redfield Comparison with Marginal Distribution Curves
ΔAlk/HPO4 2-
ΔAlk/NH4
0
50
100
150
200
250
300
0
5
10
15
20
25
30
1225
1230
1427
1426
1319
994a
995b
997a
1059a
ESAO Dist. Curve
All Other Sites Dist. Curve

Figure 11.

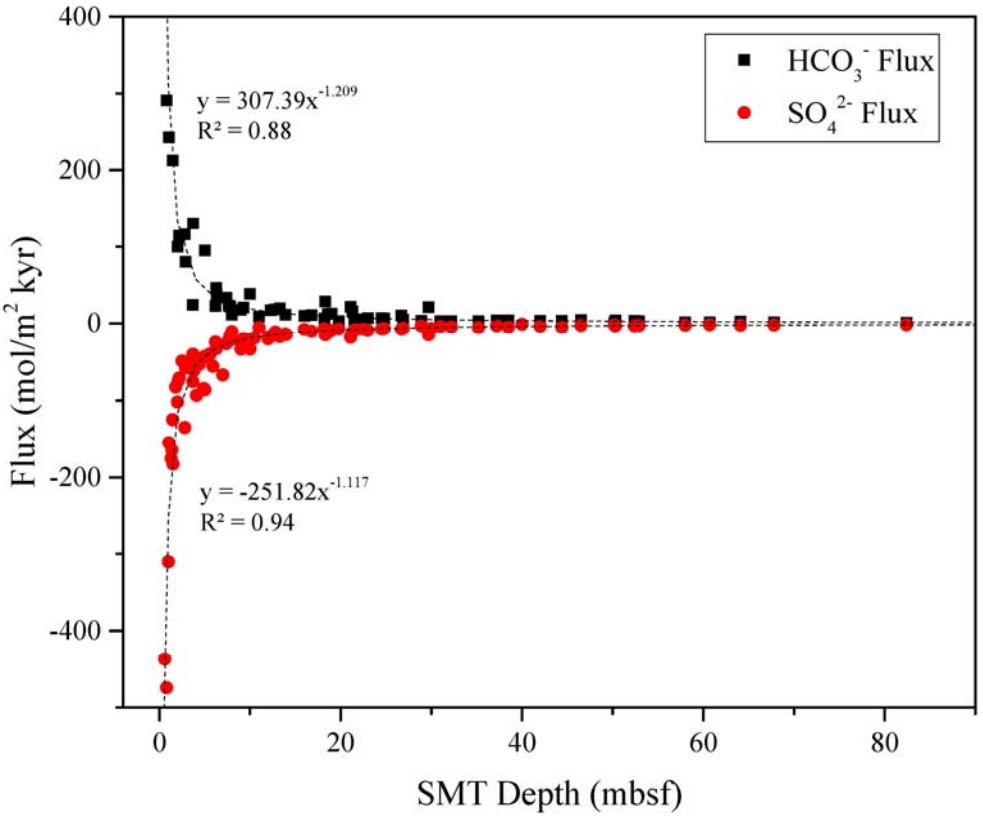
400
200
0
-200
-400
0
20
40
60
80
Flux (mol/m^2 kyr)
SMT Depth (mbsf)
HCO_3^- Flux
SO_4^{2-} Flux
y = 307.39x$^{-1.209}$
R² = 0.88
y = -251.82x$^{-1.117}$
R² = 0.94

Figure 12.

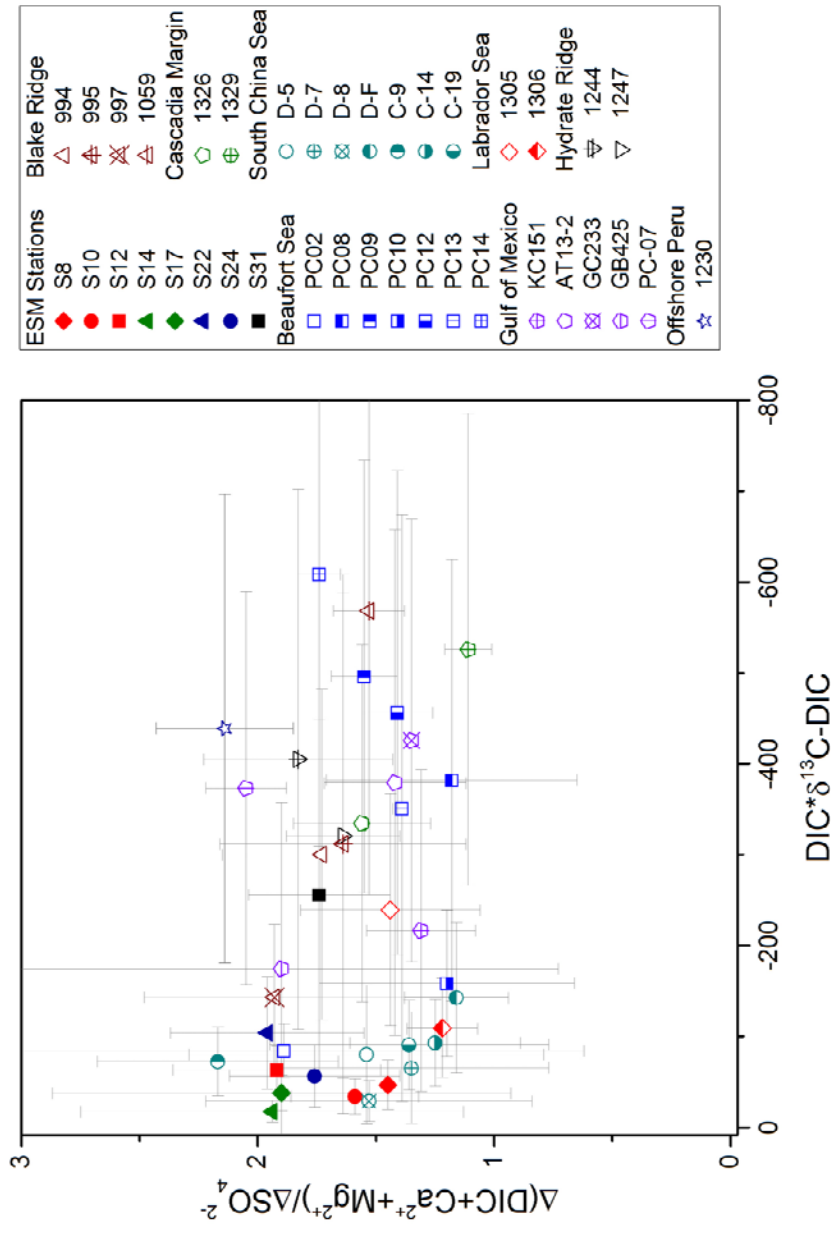
ESM Stations
S8
S10
S12
S14
S17
S22
S24
S31
Beaufort Sea
PC02
PC08
PC09
PC10
PC12
PC13
PC14
Gulf of Mexico
KC151
AT13-2
GC233
GB425
PC-07
Offshore Peru
1230
Blake Ridge
994
995
997
1059
Cascadia Margin
1326
1329
South China Sea
D-5
D-7
D-8
D-F
C-9
C-14
C-19
Labrador Sea
1305
1306
Hydrate Ridge
1244
1247
Δ(DIC+Ca2+ +Mg2+)/ΔSO4 2-
DIC*δ13C-DIC
3
2
1
0
0
-200
-400
-600
-800

82 Table 1.

Table 1 QA/QC Results

Analysis	Sample Type	Number	Result
Alkalinity	Spiked	15	PE = 1.53%
Alkalinity	Duplicate	8	PD = 1.30%
δ^{13}C-DIC	Seawater Standard	2	0.23‰ and 0.32‰
δ^{13}C-DIC	Blind Field Duplicate	4	PD = 22.98%
δ^{13}C-DIC	Field Blank	1	No Result
δ^{13}C-DIC	Duplicate	10	PD = 14.70%
Metals	Spiked	51	RSD = 2.55% (Ba), 2.17% (Ca), 1.53% (Fe), 0.77% (Mg), 1.73% (Mn), 1.88% (S), and 1.42% (Sr)
Metals	Blind Field Duplicate	11	PD = 2.56% (Ba), 3.77% (Ca), 5.81% (Fe), 2.68% (Mg), 3.07% (Mn), 0.71% (S), and 3.79% (Sr)
Metals	Field Blank	2	BDL
Phosphate	VKI Standard	2	PE = 1.28% and 2.69%
Ammonia	VKI Standard	2	PE = 2.40% and 6.25%

Notes: PE = Percent Error
PD = Percent Difference
RSD = Relative Standard Deviation
BDL = Below Detection Limit

83

84

85

86

87

88

89

90

91

92 Table 2.

Table 2 - Reported and Calculated Fluxes

Ocean	Location	Water Depth (m)	SMT Depth (mbsf)	SO_4^{2-} Flux (mol/m^2kyr)	Alkalinity Flux (mol/m^2kyr)	$\delta^{13}C$ at SMT (‰)
Arctic	Beaufort Sea - Cape Halkett[a,b]	280	1.06	-154.8	242.6	-21.5
Arctic	Beaufort Sea - Cape Halkett[a,b]	342	1.47	-124.7	212.3	-20.2
Arctic	Beaufort Sea - Cape Halkett[a,b]	1005	3.73	-44.2	130.3	-18.2
Arctic	Beaufort Sea - Cape Halkett[a,b]	1458	6.29	-27.4	46.3	-19.7
Arctic	East Siberian Slope	349	61	-1.8	1.7	--
Arctic	East Siberian Slope	367	25	-6.9	6.3	--
Arctic	East Siberian Slope	384	64	-2.4	2.3	--
Arctic	East Siberian Slope	524	35	-5.6	2.8	--
Arctic	East Siberian Slope	733	58	-2.1	1.5	--
Arctic	East Siberian Slope	977	58	-2.1	1.6	--
Arctic	East Siberian Slope	964	23	-9.2	6.8	--
Arctic	East Siberian Slope	1000	52	-3.3	3.3	--
Arctic	East Siberian Slope	1143	44	-5.1	3.5	--
Arctic	East Siberian Slope	1120	14	-13.9	11.3	--
Atlantic	New Jersey Continental Slope[q,i]	912	28.9	-3.3	3.6‡	--
Atlantic	Blake Ridge[q,p]	1293	50.3	-3.4	3.8‡	--
Atlantic	Blake Ridge[q,p]	1798	26.9	-6.6	4.9‡	--
Atlantic	Blake Ridge[q,x]	2567	42.0	-3.8	3.5‡	--
Atlantic	Blake Ridge[q,x]	2641	24.5	-7.6	6.9‡	--
Atlantic	Blake Ridge[q,x]	2777	21.7	-8.3	5.4‡	--
Atlantic	Blake Ridge[q,x]	2770	22.5	-7.8	4.7‡	--
Atlantic	Blake Ridge[q,x]	2798	21.5	-8.7	4.4‡	--
Atlantic	Blake Ridge[q,p]	2985	9.3	-20.0	20.4‡	--
Atlantic	Blake Ridge[q,p]	3481	12.3	-17.1	17.0‡	--
Atlantic	Blake Ridge[q,p]	4040	16.8	-10.5	10.8‡	--
Atlantic	Gulf of Mexico - Keathley Canyon[w]	1300	9	-33‡	17‡	-49.6
Atlantic	Gulf of Mexico - Atwater Valley[w]	1300	0.1	-2901	--	--
Atlantic	Gulf of Mexico - Atwater Valley[w]	1300	0.1	-2901	--	--
Atlantic	Gulf of Mexico - Atwater Valley[w]	1300	0.6	-437	--	--
Atlantic	Gulf of Mexico - Atwater Valley[w]	1300	7	-67	--	-46.3
Atlantic	Amazon Fan[q,v,y]	3191	37.2	-3.2	4.1‡	-39.8
Atlantic	Amazon Fan[q,v,y]	3474	6.2	-24.6	22.7‡	-47.5
Atlantic	Amazon Fan[q,v,y]	3704	3.7	-40.3	24.3‡	-49.6
Atlantic	Western Africa[q,z]	426	12.8	-12.5	18.2‡	--
Atlantic	Western Africa[q,z]	738	52.9	-3.1	2.9‡	--

Atlantic	Western Africa[q,z]	1280	21.3	-12.0	15.6‡	-19.8
Atlantic	Western Africa[q,z]	1402	18.3	-14.9	28.3‡	--
Atlantic	Western Africa[q,z]	1713	38.5	-5.1	4.1‡	--
Atlantic	Western Africa[q,z]	2179	26.7	-7.8	10.4‡	--
Atlantic	Western Africa[q,z]	2382	21.1	-18.1	21.8‡	--
Atlantic	Western Africa[q,z]	2995	29.7	-14.9	20.9‡	--
Atlantic	Argentine Basin[l]	1228	10.5	-19.1	--	--
Atlantic	Argentine Basin[l]	1492	12	-20.2	--	--
Atlantic	Argentine Basin[l]	1568	4.9	-84.6	--	--
Atlantic	Argentine Basin[l]	1789	5.9	-55.6	--	--
Atlantic	Argentine Basin[l]	3247	10	-21.8	--	--
Atlantic	Argentine Basin[l]	3167	14	-14.7	--	--
Atlantic	Argentine Basin[l]	3542	3.7	-75.4	--	--
Atlantic	Argentine Basin[l]	3551	5.6	-39.9	--	--
Atlantic	Argentine Basin[l]	3551	4.1	-93.3	--	--
Atlantic	Argentine Basin[l]	3623	5	-43.1	--	--
Atlantic	Argentine Basin[l]	4280	5.1	-43.5	--	--
Atlantic	Argentine Basin[l]	4799	12	-17.9	--	--
Indian	Oman[q,1]	591	50.2	-2.2	1.1‡	--
Indian	Oman[q,1]	804	46.5	-2.8	4.4‡	--
Indian	Oman[q,1]	1423	82.4	-1.8	0.8‡	--
Pacific	Bering Sea[p,2]	1008	6.3	-32.8	37.8	-25.1
Pacific	Cascadia[q,u,2]	959	9.0	-23.6	--	-23.8
Pacific	Cascadia[q,u,2]	1322	7.9	-21.3	--	-30.8
Pacific	Cascadia[q,u,2]	1828	2.5	-49.0	--	-33.9
Pacific	Cascadia - Hydrate Ridge[o]	834	8	-10.9	11.3	-19.6
Pacific	Cascadia - Hydrate Ridge[o]	850	7.65	-22.3	23.2	-30.2
Pacific	Cascadia - Hydrate Ridge[o]	871	7.4	-26.6	33.4	-24.9
Pacific	Cascadia - Hydrate Ridge[g]	896	7.8	-16	22	-22.5
Pacific	Umitaka Spur[h]	900	2.2	-71	114	--
Pacific	Umitaka Spur[h]	947	2.9	-58	80	--
Pacific	Umitaka Spur[h]	1034	2.0	-102	100	--
Pacific	Japan Sea[s,4]	901	10	-33.6	38.4‡	--
Pacific	California Margin[q,5]	955	13.3	-17.3	19.6‡	--
Pacific	California Margin[q,5]	1564	19.0	-9.3	12.8‡	--
Pacific	California Margin[q,5]	1926	31.0	-4.3	3.1‡	--
Pacific	Nankai Trough[q,6]	1741	32.2	-4.9	3‡	--
Pacific	Nankai Trough[s,6]	2997	11.0	-5.6	8.7‡	--
Pacific	Nankai Trough[q,6]	3020	18.2	-7.0	6.4‡	--

Pacific	Santa Barbara[k]	587	1.3	-175.2	--	--
Pacific	Soledad[k]	542	1	-310.3	--	--
Pacific	Pescadero[k]	408	1.4	-164.3	--	--
Pacific	Magdalena[k]	600	1.5	-182.5	--	--
Pacific	Alfonso[k]	713	0.8	-474.5	--	--
Pacific	Costa Rica Margin[q,7]	3306	16.0	-8.1	9.6‡	--
Pacific	Costa Rica Margin[q,7]	4177	19.8	-7.5	3.1‡	--
Pacific	Costa Rica Margin[q,7]	4311	18.6	-12.3	12.4‡	--
Pacific	Peru Margin[s,8]	161	30	-6.9	--	--
Pacific	Peru Margin[t,9]	427	40	-1.2	--	-25.4
Pacific	Peru Margin[t,9]	5086	9	-25.0	--	-13.2
Pacific	Chilean Coast[c]	586	5.55	-22.9	--	--
Pacific	Chilean Coast[c]	723	0.33	-362.0	--	--
Pacific	Chilean Coast[c]	980	2.92	-45.3	--	--
Pacific	Chilean Coast[c]	768	10.11	-13.3	--	--
Pacific	New Zealand - Porangahau Ridge[f]	1900-2150	12.8	-11.4	--	-31.4
Pacific	New Zealand - Porangahau Ridge[f]	1900-2150	4.4	-53.3	--	-31.6
Pacific	New Zealand - Porangahau Ridge[f]	1900-2150	3.6	-50.5	--	-31.4
Pacific	New Zealand - Porangahau Ridge[f]	1900-2150	2.1	-74.2	--	-33.4
Pacific	New Zealand - Porangahau Ridge[f]	1900-2150	3.8	-61.5	--	-35.0
Pacific	New Zealand - Porangahau Ridge[f]	1900-2150	1.8	-82.6	--	-48.8
Pacific	New Zealand - Hikurangi[b,d]	350	39.5	5‡	7.3‡	--
Pacific	New Zealand - Hikurangi[b,d]	332	12.9	19.3‡	13.6‡	--
Pacific	New Zealand - Hikurangi[b,d]	98	0.87	192.1‡	160.9‡	--
Pacific	New Zealand - Hikurangi[b,d]	285	3.64	65.2‡	59.6‡	--
Southern Ocean	Antarctic - Cumberland Bay[n]	237	5.03	-86	95	-25.4
Southern Ocean	Antarctic - Cumberland Bay[n]	260	0.80	-539	291	-23.5
Southern Ocean	Antarctic - Cumberland Bay[n]	275	2.80	-135	116	-15.5